C.P. No. 701

MINISTRY OF AVIATION

AERONAUTICAL RESEARCH COUNCIL

CURRENT PAPERS

Excitation Temperature Measurements of Gases in an Arc-Heated Wind Tunnel at 1.3×10^{-2} Atmosphere, using Relative Intensities of Spectral Lines

By

B.D Adcock and W.E.G. Plumtree,
Department of Aeronautics,
Imperial College

LONDON: HER MAJESTY'S STATIONERY OFFICE

1965

PRICE 13s 0d. NET

C.P. No. 701

Excitation Temperature Measurements of Gases in an Arc-Heated Wind Tunnel at $1 \cdot 3 \times 10^{-2}$ Atmosphere, using Relative Intensities of Spectral Lines

- By -
B. D. Adcock and W. E. G. Plumtree,
Department of Aeronautics,
Imperial College

Communicated by Prof. P. R. Owen

April, 1963

SUMMARY

A description is given of a method for obtaining temperatures of gases by spectrogrammetric measurements of the relative intensities of spectral lines, applied to the gas in an arc-heated wind tunnel ('plasma-jet').

Qualitative details of impurities present in the wind tunnel are discussed.

An explanation starting from basic principles, concerning line spectra and relative intensity measurements, is designed for the benefit of technologists having only a general background knowledge of physics.

A comprehensive compilation of transition probabilities and other relevant data for neutral and first-stage ionization argon lines, is included as an Appendix.

List/

Replaces A.R.C. 24 689.

List of Contents

9./

---

1. The Arc-Heated Wind Tunnel ('Plasma Jet')

1.1 Description of the tunnel

An arc-heated wind tunnel, which operates at reduced pressures, has been fully described in Ref. 1. It should suffice to indicate the principle of its operation, and reference to Fig. 1 should assist the following explanation. A high current arc heats a stream of inert gas which is forced through the gap between the electrodes. The arc discharge produces a region of ionized gas* between the conical cathode and the cylindrical anode, and the high temperature produces a considerable expansion of the gas. The heated gas accelerates along the axis of the anode to the 'plenum chamber' (the latter

is/

* An ionized gas is termed a 'plasma' - hence the name 'plasma-jet' for this type of arc.

is intended to assist the heterogeneous gas to enter a steady state). A 'convergent-divergent nozzle' forms the exit to this chamber and the hot gas emerges through the nozzle with a high velocity (3 000 m s^{-1} or 9 000 ft s^{-1})*.

The properties of this high velocity jet can be investigated at low ambient pressures, and for this, a large continuously evacuated vessel is required to surround the jet. Since the wind tunnel normally operates with the pressure in this vessel about 5 to 15 torr (mm Hg), or 6×10^{-3} to 2×10^{-2} atm, the path length of the emerging jet extends some 25 cm (10 in.) beyond the exit of the nozzle. The somewhat unexpected extent of this region of excited gas is probably to be explained by the presence of meta-stable states** of the atoms[3], since, in the presence of traces of hydrogen, or with helium as the working fluid, the volume of excited gas is smaller. The production of such regions of radiation from an argon jet under very similar conditions to those just described, is explained in a recent research note by Brewer and McGregor[4]. Further discussion of this effect is to be found in Section 7.2 of this report.

1.2 Measurements in hot gases

The combination of high velocity and high temperatures presents some difficulty in the determination of the physical properties of the gas, and advanced techniques must be employed (e.g., widths of spectral lines, infra-red techniques, and other spectroscopic methods[5]; microwave analysis; interferometric measurements; Langmuir probes, etc.).

It was decided to investigate the possibility of measuring temperatures using spectrographic techniques, which generally involve the determination of the intensity or the profile of selected spectral lines. In this case, it is the relative intensities of the lines in a given spectrum that are investigated.

2. The Significance of "Temperature"

The simple concept of the temperature of a mass of fluid can no longer be applied to a gas at high temperature. The 'temperature' measured by a method directly involving the translational energy of atoms, say, will not necessarily agree with the value measured by another method involving ionization parameters - even though both methods can be based on accurately known principles of physics. Such 'temperatures' will be equivalent only under the admittedly elusive conditions of thermal equilibrium in a hot gas at low pressure[6,7].

For/

---

* British Standards/International abbreviations for units are used in this report (see Ref. 2).

** A term which is explained in Section 3.2.

For a monatomic gas the translation temperature, excitation temperature*, ionization temperature** and electron temperature*** may be quoted. Similarly, for a partially dissociated diatomic gas, the translation, vibration, rotation, excitation and ionization temperatures may be selected as applicable to the relevant problem.

Surveys of the production and measurement of different classes of temperature[8,9], and a résumé of some value in the appreciation of the applicability, or otherwise, of thermal equilibrium properties in arcs[6], may be consulted for further information on this subject.

The current programme of research has been initiated by an attempt to measure excitation temperatures in the case where argon is used as the working mediu

3. The Emission of Light from Atoms

3.1 Energy levels

For the purposes of this application the pictorial Bohr-Sommerfeld model of the atom is adequate. Electrons in an atom may be visualized simply as occupying certain stable, elliptical orbits about the nucleus (see Fig. 2). When the internal energy of an atom is raised (e.g., by a collision with another atom) an electron transfers to an orbit corresponding to a higher 'energy level'. A limited number of discrete energy levels are available to such an electron, and the ultimate choice in a particular case is dependent upon the quantity of energy received.

Fig. 3 shows schematically the energy levels available to such an electron. The three columns on the left show the energy levels of an atom of a given element (here, quite fictitious) in the case where energy is incident, and the columns on the right show a subsequent stage which is described in Section 3.2. An electron generally transfers from one column to an adjacent column (a condition termed in atomic spectral theory "$\Delta\ell = \pm 1$")****. Transitions rarely occur between energy levels in any one column (i.e., "$\Delta\ell \neq 0$").

The three columns on the left of Fig. 3 represent an atom receiving either a quantity of energy ϵ_1, or another, ϵ_2. By the laws of quantum physics,

the/

---

* The excitation temperature is derived from measurements of the intensity of radiation from excited atoms. This is sometimes termed 'electronic excitation temperature', but the electrons concerned are not deemed to be 'excited' - it is the atoms which are excited. Another term is 'population temperature'.

** The ionization temperature is derived from measurements of the relative population levels of ionized and neutral atoms.

*** The electron temperature is derived from measurements of the intensity of continuum radiation from atoms suffering collision by free electrons, if the latter are present in the gas. It is an indication of the energy distribution of the free electrons.

**** ℓ is known as the 'azimuthal quantum number' and has integral values 0,1,2,3, ... which are respectively allocated to the columns of energy levels (see Ref. 64).

the quantity of energy received for a particular energy level transition, is completely characteristic of that transition, and no other amount of energy can be donated to cause that transition - of course, the appropriate amount of energy might be extracted from a larger quantity of incident energy.

When an electron has attained an upper energy level, the atom is said to be in an "excited state", since the atom is tending to eject the extraordinary additional energy at the first opportunity.

3.2 Stability of "excited states"

An electron does not remain in these upper, atomic 'excited state' levels, but returns to a lower level, generally after a mean period of about 10^{-8}s. Energy is emitted in the form of radiation when this process occurs. As demonstrated in Fig. 3, this transition of the electron need not return the atom to its original state (i.e., the final level shown is not the level, prior to excitation, depicted on the left of Fig. 3). This necessarily implies that the quantity of energy ejected in this example need not be the same as the previously incident energy. The terminology shown in this diagram for the ejected energy will be discussed in later sections.

In the case of some high energy levels, the atom may remain in the excited state for much longer periods before an event occurs which allows an otherwise improbable transition to a lower level to take place. Such an excited state is termed a 'meta-stable state'.

3.3 Properties of a transition

In general, there are a number of levels available, between which transitions may occur, but the total number of energy levels is limited, since only certain discrete quantities of internal energy are allowed to exist within the atom (i.e., only certain fixed 'orbits' are allowed for the electrons, as seen previously in Fig. 3). In spite of this limited allocation of energy levels, there can be no certainty in predicting which two levels will be involved in a transition at any particular instant. Fortunately, it is possible to evaluate experimentally a probability that a given transition will take place, relative to other possible transitions.

The quantity of energy emitted by a particular transition has a magnitude associated with the actual energy levels involved, and is characteristic of that transition (again shown in Fig. 3). The energy emitted from a given atom undergoing such a change, is in the form of a pulse of light or other electromagnetic radiation, and since the quantity of energy is completely defined in the given case, this light has one particular frequency associated with that particular transition*.

3.4 The many-lined spectrum

A large number of atoms, each in different groups of states, will radiate pulses of light with certain 'selected' quantities of energy (i.e., with

certain/

---

* This statement is still valid even if external influences, such as high collision rates with surrounding particles - producing 'collision broadening', cause the frequencies of photons to vary slightly. In such cases, the corresponding energy levels in a particular atom may be considered to have been altered accordingly.

certain frequencies) depending upon the states involved, and a line spectrum results if the light is collected in a spectrograph. The intensity of a given line will partly depend upon the population of its corresponding atomic state, relative to the total homogeneous population of atoms. The probability associated with each transition, which has been mentioned in the previous section, is another principal factor governing the intensity of a given line, and is called the transition probability (A). It is equivalent to the reciprocal of the mean lifetime of the particular excited state of the atom, before the decay to the appropriate lower level. (See Section 4.2 for a full statement on the intensity of a spectral line.)

3.5 "Excitation temperature"

The types of transitions occurring in a gas will depend upon the initial input of energy to the atoms, and the relative intensities of the resulting radiated frequencies allow a concept of a 'temperature' to be formulated. This 'excitation temperature' can generally be considered to be a close indication of the translation temperature of the gas, since inter-atomic collisions are mainly responsible for the excitation, at least in the case where temperatures are not high enough to permit a high concentration of free electrons*. Agreement of the excitation and translation temperatures will occur under conditions of thermal equilibrium in the gas, and the basic requirement for this aspect of the term 'thermal equilibrium' is that the mean free paths of the atoms should be short enough to allow a reasonably high frequency of inter-atomic collisions.

3.6 Self-absorption

A possible source of error in this treatment is connected with the fact that the light so emitted can be absorbed by atoms of the gas in the cooler regions through which the light will generally pass. This obviously affects the measured intensity ratios of the selected spectral lines. In the particular case of those lines investigated in these experiments, this effect is known to be small[10]. An experimental verification of the degree to which it affects these lines is now in progress.

4. The Derivation of "Excitation Temperature" from Relative Intensities of Spectral Lines (Ref. 11)

4.1 The Maxwell-Boltzmann law (Ref. 12)

Consider the atoms in a given volume of homogeneous gas in thermal equilibrium. Allocate some of the atoms to a number of upper energy levels (i.e., different states of excitation), while allowing others to remain unexcited at the particular instant chosen.

Let there be

N_a atoms with an electron at energy level a,
" " " " " " " ,
N_m " " " " " " " m,
N_n " " " " " " " n,
" " " " " " "

Consider/

---

* Free electrons can be present in a gas when ionised atoms of either the gas or an impurity are in the vicinity. They collide with atoms and excite the latter, thus producing more excitation radiation.

Consider the m and n states. Then assuming that the relative numbers of atoms in these states are given by the Maxwell-Boltzmann law of distribution:

$$N_m/N_n = (g_m/g_n) \exp(- E_{nm}/kT) \qquad \ldots(4.1)$$

where g is the 'statistical weight' for the specified levels*,

E_{nm} is the energy difference between the two levels,

k is Boltzmann's constant,

and T is the excitation temperature.

4.2 The intensity of a spectral line

Now the intensity of light emitted at a frequency ν (i.e., from a particular transition) is proportional to the number of atoms N_E in the corresponding upper state with energy E, to the discrete energy of the 'photons'** constituting this light, and to the transition probability A described above. Since the energy of a photon is given by $h\nu$, where h is Planck's constant, then the intensity is given by:

$$I = K'N_E A \cdot h\nu \qquad \ldots(4.2)$$

where K' is a constant of proportionality.

Note that the value of A depends upon the particular transition involved, and hence upon ν, the frequency of the corresponding radiation.

4.3 Relative intensities

Consider now two of the many different transitions occurring in the volume of gas referred to in Section 4.1. One of the transitions is considered to be from level m to some lower level, say d, and the other from level n to a lower level, say f (see Fig. 4). Let the 'm' transition produce a photon with frequency ν_m*** and the 'n' transition, one with frequency ν_n. Then taking equation (4.2) and inserting transitions 'm' and 'n' respectively:

$$I_m = K'N_m A_m \cdot h\nu_m$$

$$I_n = K'N_n A_n \cdot h\nu_n.$$

Using/

---

* The statistical weight of a given level expresses the probability of an atom attaining that level. In the theory of atomic states $g = 2J + 1$. J is the total 'angular momentum' of an atom with a given electronic 'structure'. Values of g are tabulated in Appendix II, for useful argon lines.

** A 'photon' is the pulse of light mentioned in Section 3.3, possessing an energy and frequency dependent upon the particular transition producing it. Expressions for transition probabilities, in terms of other parameters, may be found in Ref. 13.

*** Strictly, these suffices should be md and nf, but since no confusion is inherent, they are abbreviated to m and n in this paper.

Using both equations, and substituting from equation (4.1):

$$\frac{I_m}{I_n} = \frac{N_m}{N_n} \cdot \frac{A_m}{A_n} \cdot \frac{\nu_m}{\nu_n} = \frac{A_m}{A_n} \cdot \frac{\nu_m}{\nu_n} \cdot \frac{g_m}{g_n} \exp\left(-\frac{E_{nm}}{kT}\right). \qquad \ldots(4.3)$$

Taking logarithms:

$$\log (I_m/I_n) = \log (g_m A_m \nu_m / g_n A_n \nu_n) - (E_{nm}/kT) \log e. \qquad \ldots(4.4)$$

This is an equation of the form $Y = C + mX$

where $X = 1/T$,

gradient $m = -(E_{nm} \log e)/k$,

and intercept $C = \log (g_m A_m \nu_m / g_n A_n \nu_n)$.

4.4 An alternative approach (Ref. 11)

Instead of attempting measurements using individual pairs of lines, as required by the above treatment, a neater method of computation is preferable, which allows the mean result for a number of lines to be derived. At the same time, it demonstrates the reliability, or otherwise, of the values of the transition probabilities employed (see Section 10.4 and Fig. 11).

As in Section 4.2, consider a particular spectral line with a corresponding upper energy level E and transition probability A, and apply the consequences of assuming that the number of atoms in the energy state E is given by the Maxwell-Boltzmann law of distribution of energy among the total number of atoms.

Equation (4.2) now becomes:

$$I = K' A h\nu \cdot N_E = (K' A h\nu N g/U) \cdot \exp(-E/kT) \qquad \ldots(4.5)$$

where U is the 'partition function' or sum of the statistical weights of all the states present in the atoms of the gas,

and N is the total number of atoms present.

Now the factors K', h, N and U do not depend upon the energy E of the emitting atom, therefore put $K = K'h N/U$. Thus,

$$I = K g A\nu \cdot \exp(-E/kT) \qquad \ldots(4.6)$$

i.e., $$\log (I/Kg A\nu) = -(E \log e)/kT. \qquad \ldots(4.7)$$

A graph of $\log (I/g A\nu)$ as ordinates and E as abscissae should thus be a straight line of slope $-(\log e)/kT$.

4.5 The choice of units

As pointed out in Ref. 11, from which this treatment has been derived, the system of units to be employed, in either of these computational methods,

is quite arbitrary. The only limitation applies to the units for kT and E, which must be compatible. Values of E are available in tables in terms of wavenumbers (Ref. 14 and Appendix II), which are known more accurately than any conversion factor to electron-volts (eV). This is an important consideration, since small differences in values of E are employed in this treatment. If E is expressed in electron-volts to only two places of decimals, as in some of the literature, gross errors can result in the differences.

For computations using wavenumbers, the value for k is given by:

$$k = 0{\cdot}69502 \text{ cm}^{-1} \text{ (deg K)}^{-1},$$

assuming that T is expressed in degrees Kelvin. The corresponding value for (log e)/k is thus

$$(\log e)/k = 0{\cdot}62487 \text{ cm deg K.}$$

It would be consistent to use values of ν in wavenumbers too, but generally tables are available only in wavelengths. However, it is quite possible to use wavelengths in these equations, since there is only a constant of proportionality involved in the conversion. Equation (4.4) becomes:

$$\log (I_m/I_n) = \log (g_m A_m \lambda_n / g_n A_n \lambda_m) - (E_{nm}/kT) \log e \qquad \ldots(4.8)$$

and equation (4.7) becomes

$$\log (I\lambda/KgA) = - (E_{(n)} \log e)/kT. \qquad \ldots(4.9)$$

Values of g are obtained from tables of the corresponding values of J in Ref. 14, since g = 2J + 1. However, values of not only g, but also E, A, gA and log (λ/gA)* for a large number of ArI and ArII lines are tabulated in Appendix II to this paper.

Some difficulty may be experienced in choosing the best straight line through the plot of experimentally derived points. This is to be expected when transition probabilities are doubtful. A statistical theory is described in Appendix III by which the gradient of the best fitting straight line can be computed.

5. The Measurement of Line Intensities

5.1 Detection methods and their comparative advantages

Two alternative methods for recording the intensities of spectral lines were considered - photographic and photoelectric, the latter method being acknowledged to present fewer experimental hazards than the complex photographic densitometric technique. However, since a substantial number of lines were to be compared for each temperature determination, corresponding to a given set of operation conditions, and the time required for each determination had not to be inconveniently long, it was decided that the photographic method still offered some advantages over the use of a photomultiplier detector. The convenience of the photographic plate as a compact record of several experiments was also deemed an advantage. Both methods require the use of large quantities of recording

chart,/

---

* The usefulness of this factor should be stressed; the common logarithms of the relative intensities are simply added to these corresponding factors to obtain the required ordinates for Section 4.4.

chart, in one case for recording the photomultiplier current, and in the other for recording line image densities on the micro-densitometer. Computations in photographic densitometry are based on empirical techniques, and the methods used are described later in Section 5.4 and Appendix I. A further survey of the methods available is published in the A.S.T.M.* publications[15].

It is known that the arc-heated gas stream is not always formed continuously, but is subject to high-frequency perturbations causing fluctuations in temperature, pressure, radiation, etc.[16,17]. The photographic emulsion naturally records the mean effect of these variations over exposure times lasting about 2 to 20 s.

5.2 The photographic method

It is in general desirable, from the point of view of the accuracy of the experimental measurements, to compare spectral lines of closely similar intensities (currently the argon blue group - see Section 7.4) and such work demands the use of a sensitive discriminating detector. For this reason, slow photographic plates of medium to high contrast were chosen in order to detect the small intensity differences with greater accuracy. The Ilford N.50 thin-film, half-tone plate was employed initially, although the contrast is a little high in that it is sometimes difficult to judge the exposure time accurately enough to be able to compare the strongest and weakest argon blue lines on the same spectrogram. For this reason the Ilford N.30 ordinary plate is now extensively employed in this project.

Plate characteristics, which must be considered when selecting an emulsion for a particular spectrographic purpose, are set out in the first part of Appendix I.

The blackening density of a photographic plate is measured by a photoelectric instrument termed the microdensitometer, which measures the transmittance T of a particular line by comparing the intensity of the analysing light beam transmitted by that line to the intensity transmitted through an adjacent clear portion of the emulsion. This latter value is set as T = 100%, and zero is set with the analysing light beam cut off.

To obtain a true measure of the intensity of a spectral line, it is necessary that the spectrograph slit shall be at least as wide as the broadest line to be examined. This ensures that the densitometer trace has a flat-topped profile, having the advantage that the height of the plateau alone is proportional to the intensity, so removing the necessity of integrating the trace image area, see Harrison[18]. In these experiments a slit width of 50 μm (micrometre), or 0·002 in., was used.

It is general practice, when obtaining a densitometer trace of a spectral line, to employ a densitometer slit width about one-third that of the spectrograph slit. This criterion minimizes the effects of diffraction. The scanning speed of the instrument must be chosen such that the true line profile is fully recorded, whilst minimizing the effect of the emulsion granularity.

5.3/

* The American Society for Testing Materials - an American equivalent to the British Standards Institute.

5.3 Spectrogrammetric measurements

5.3.1 Plate calibration

The degree of blackening of a photographic emulsion is a function of the quantity of incident radiant energy and of the development process. In order to obtain a measure of the relative intensity* of the incident light for a particular spectral line it is therefore necessary to calibrate the plate in two ways:-

(a) To enable determination of the variation of apparent recorded density with the incident energy, i.e., intensity calibration, and

(b) To allow for the variation of the wavelength response of the emulsion, i.e., colour calibration.

5.3.2 Intensity calibration and characteristic curves

The density of the blackening of a photographic plate is defined as

$$D = -\log_{10} T$$

where T is the fractional transmittance of a spectral line, as measured by the microdensitometer.

If the quantity of radiant energy is varied within a series of exposures identically developed, then a plot of log exposure against D will be similar to Fig. 5 for any emulsion. Such a plot is termed a characteristic curve, or, in some literature, the H and D curve (Hurter and Driffield, 1890). Thus if the exposure can be varied by known steps such a curve may be plotted. This will permit determination of the actual relative intensities** of the resulting images as a function of measured density of the images, along the straight line portion of the curve. The slope of this straight line portion of any characteristic curve, using $D(T)$ or any other function of T, is termed the gamma, γ, of the emulsion.

5.3.3 Intensity calibration technique

A variety of suitable means are available for impressing upon the photographic emulsion a series of density steps of known differential increments***, and these steps may be plotted logarithmically as the abscissa of a characteristic curve against a function of transmittance as ordinate. In practice, all the available steps may be employed, or, alternatively, only two may be considered ("two-step" technique, Ref. 15). The latter has the advantage that the effect of any non-uniformity of the vertical illumination of the spectrograph slit is

minimized/

---

* The expression "relative intensity" indicates that the intensities of the various spectral lines are not determined on any absolute scale, but are merely quoted as being relative to any given line.

** The expressions "exposure" and "relative intensity" are only interchangeable provided certain precautions, to be enunciated below, are observed, particularly with regard to reciprocity failure.

*** A brief summary of available technique is included in Appendix I; in this work we have employed a Hilger seven-step, evaporated rhodium-on-quartz filter.

minimized (Doherty[19], considers this to be an important point), although this must be offset against the greater chance of error in measuring only two values of transmittance. The vertical uniformity may be checked by comparing the transmittances originating from the clear strips above and below the filter for any line, and the effect of non-uniformity may be partly negated by inverting the filter and repeating the exposure.

5.3.4 The practical determination of contrast

The quantity of incident radiant energy is a function of the intensity of the radiation I, and of the exposure time t, but it is not true to state, however, that it is equal to the product It. An exposure of 10 s to a radiant flux of 1 μW ster^{-1} cm^{-2}* will not in general give the same density as an exposure of one second to a flux of 10 μW ster^{-1} cm^{-2}. This effect is termed reciprocity failure. (See, for example, Chapter 7 of Ref. 18, and Ref. 20.)

The value of γ further varies with development technique, i.e., developer composition, freshness, temperature, agitation and development time, the latter variation being indicated by Fig. 6. It should be remembered that overdevelopment gives rise to possible fogging where there has in fact been no exposure to light.

From experience it is found that the value of γ cannot in practice be held constant for those emulsions used in our research, however carefully the development process is controlled, and it becomes necessary to calibrate not only each spectrogram but each spectral line of interest within the spectrogram. Furthermore, whatever the degree of agitation during development, it is not possible to entirely prevent a decrease in developer strength in the close proximity of a strongly exposed line. This dilution stimulates the Intensity Retardation of Development (IRD) effect[21] which causes strong lines to have smaller gammas than weaker lines in the same region of the given spectrogram.

Lack of sufficient agitation during the development process can have more serious consequences than merely enhancing the IRD effect. If the local dilution of the developer is very marked, it will cause the tails of the line profile to be severely underdeveloped, giving rise to considerable doubt when estimating the position of the 100% T mark, and it may further cause a dip in the peak of the profile of a strong line. These phenomena, collectively termed the Eberhard effect, render very difficult an accurate determination of the transmittance. A recommended method for reducing these effects to a minimum is to brush the plate gently while development proceeds. Brushing the plate in one direction only, however, gives rise to profile distortion.

Because of the IRD effect it has been our practice to measure γ for each line to be analysed and to employ this value in subsequent calculations, thus allowing for the degree of randomness in gamma.

Throughout this work we have used the Seidel function $\Delta(T)$ in place of the density $D(T)$; this is explained fully in Appendix I.

5.3.5 Colour calibration

The relative wavelength response of the emulsion was determined using a standard tungsten ribbon lamp in place of the test source, employing otherwise identical collecting optics and spectrograph settings. A typical variation of

transmittance/

* The abbreviation 'ster' is used to indicate a steradian, or unit solid angle.

transmittance with wavelength is indicated in Fig. 7. Using the two-step technique, a continuous variation of γ with wavelength throughout the range of interest was plotted*. A typical curve of this function is also shown in Fig. 7.

From such data, a curve was plotted (curve B, Fig. 8) of the relative intensity received at the plate as a function of λ (determined from the transmittance reading by the method of intensity calibration described in Section 5.3.2). The energy output of the standard lamp is known absolutely from the maker's calibration of lamp current as a function of true filament temperature, and from the tables of de Vos[22] for the emissivity of tungsten as a function of temperature. A typical plot of the energy output of the lamp is shown by curve A, Fig. 8.

From this figure, the ratio of curve A to curve B yields a correction factor θ as a function of λ, by which all values of relative intensity, determined from the characteristic curve (see Section 5.3.2), must be multiplied in order to correct for colour response. It is worthwhile tabulating $\log \theta$ against λ for each useful combination of wavelength range, collecting optics, spectrograph setting and emulsion employed, if routine measurements are contemplated.

5.3.6 The determination of relative intensities

In practice, we have measured the transmittances for two steps of each line, preferably one above and one below 50%T, to minimize the errors when transferring from transmittance to the Seidel function Δ. At the same time, we have endeavoured to use step pairs which are not greatly separated for each line, to minimize the effect of non-uniform vertical illumination. It is important to note further, that errors in determining transmittance resulting from fluctuations of the 100%T setting on the densitometer, or from the presence of latent background, decrease with T.

Gamma is determined from two steps using the relation:

$$\gamma = \frac{\Delta_u - \Delta_\ell}{d}$$

where Δ_u and Δ_ℓ are the Seidel functions for the upper and lower steps respectively,

and d is the step filter density increment for those steps at that wavelength.

In view of the fact that some lines may possess substantially differing intensities, necessitating the use of different step pairs, the obtained values of Δ must be corrected to those appropriate to some common step Δ_c, and these values used to calculate the relative intensities of the lines.

Thus we have

$$\log I_{rel} = \Delta_c/\gamma.$$

To/

---

*The values of γ thus obtained from the continuum will not, in general, correspond to the values obtained from line spectra at the same wavelengths, and should not be used for intensity calibration of line spectra.

To correct for colour response, I_{rel} must be multiplied by the factor θ (Section 5.3.5). It then follows that:

$$\log I = \log I_{rel} + \log \theta$$

where I is the final corrected "relative intensity" parameter to be employed in temperature calculations.

6. The Spectrograph

6.1 Choice of spectrograph

Preliminary investigations of the argon spectra produced by the radiation from the wind tunnel, operating with an unobstructed stream of the heated gas at the nozzle exit, were undertaken with medium dispersion quartz prism and glass prism spectrographs. These instruments were generously loaned by both the Chemical Engineering and Physics Departments of Imperial College. The spectra obtained indicated that the argon lines in the blue region were free of any serious interference from impurity lines, although the molecular bands arising from the presence of nitrogen in the atmosphere around the nozzle exit were very prominent in the near ultra-violet.

Measurement of the relative intensities of the argon blue lines was attempted and consistent results appeared to be possible. Nevertheless, some of the lines in the argon spectrum were insufficiently resolved by these medium dispersion prism instruments. Higher dispersion is further beneficial, in that a wide slit can be used with advantage without producing the overlapping of lines which would occur if this method were to be attempted at lower dispersions (see Plate 4).

Diffraction grating spectrographs can be considered for such an application, especially if the optical system employed in the design is such that accurate images of the slit are rendered on the photographic plate (i.e., the spectrograph is described as 'stigmatic'). A plane grating, mounted according to the principle of the 'Ebert' design[23], is most appropriate. An alternative choice in favourable circumstances would be the construction of a spectrograph with a plane grating mounted in the 'Littrow' manner[18].

The instrument selected for this work is the Bausch & Lomb 'Dual Grating' spectrograph (see Plate 2). The two gratings - each having a different blaze characteristic* and a different dispersion - are mounted in the Ebert fashion, with a large concave mirror forming the other basic unit in the optical system (see Fig. 9). Manipulation of the instrument is greatly simplified by extensive electrical control. An electronic process timer has been added to the shutter mechanism and supervision of the spectrograph has been reduced appreciably, allowing priority to be given to the more demanding requirements for the control of the wind tunnel.

The first-order spectrum obtained from the high dispersion grating (1200 lines per mm) produces a spectrogram on a 10 in. plate which conveniently

covers/

---

* Diffraction gratings which are so made that they selectively distribute the dispersed light of one particular band of frequencies into a particular 'order', are called blazed gratings. They are said to be blazed for that particular band of frequencies (see Ref. 24).

covers the region of principal interest, namely 3 700 A to 4 700 A, i.e., a dispersion of 4 A mm^{-1}. The focal plane of this spectrograph is flat, and normal thickness glass photographic plates can be used.

6.2 Mounting

A massive reinforced concrete block, supported on anti-vibration spring mounts, acts as a vibration dampening device upon which the spectrograph can be manoeuvred (see Plate 1). Such precautions are essential when a high dispersion spectrograph is used in a building containing the compressors and machinery associated with several large wind tunnels.

In order to facilitate removal of the spectrograph during periods of maintenance, a robust trolley was designed to support the instrument. This trolley is positively located on the concrete block by a vee- and flat-rail system so that the spectrograph can be replaced accurately in the working position.

After setting the spectrograph into the working position, the utmost caution must be employed to ensure that the optical components are correctly aligned. Only then can the slit be evenly illuminated and the characteristics of the image on the plate be fully representative of the source. Full details of procedures adopted to align the components of a spectrograph are described in the A.S.T.M. publications[15].

7. Qualitative Analysis of the Spectra

7.1 Impurities resulting from air leaks

Some examples of spectrograms obtained from the wind tunnel, operating with argon as the working medium, are shown in Plates 3, 4 and 5. The second positive nitrogen bands are prominent in the near ultra-violet, being emitted by the atmosphere surrounding the emerging jet of argon. The static pressure in this region was generally about 8 torr (mm Hg), or 10^{-2} atm, the actual value depending upon the flow input of argon (e.g., 4 torr for a mass flow rate of argon of 70·3 g min^{-1}, or 0·155 lb min^{-1}, at low power rating, increasing to 12 torr for an input of 99·0 g min^{-1} or 0·218 lb min^{-1} at the high power rating). Air leaking into the working section of the wind tunnel caused the appearance of these nitrogen bands and produced other impurity spectra, the most obvious components being hydrogen*, oxygen, NH and OH, so that any 'bremsstrahlung continuum radiation' that might otherwise have been detected, was masked by the impurity band-spectra. These spectra could be largely suppressed by admitting argon directly into the working section, but the effect of these impurities on plates suitably exposed for densitometric measurement of Ar I lines was negligible, and the inert atmosphere was not considered to be necessary.

7.2 Metastable states of argon (defined in Section 3.2)

The fact that only the second positive system of bands is prominent in the nitrogen spectrum from a source of this nature, has been discussed recently by Brewer and McGregor[4], and it confirms the impression that metastable states of argon atoms are prevalent in such operating conditions as those occurring in a plasma jet at reduced pressure. Metastable states are quenched by traces of hydrogen, and the visible extent of the hot gas jet should thereby be reduced.

7.3/

* The hydrogen lines are notably narrow, and absence of widening indicates that the source is in the surrounding atmosphere and not in the hot gas.

7.3 Electrode material

Since the arc electrodes consist of tungsten-tipped copper and copper respectively, it would be natural to expect the presence of copper lines in the spectra. The sensitive* resonance lines at 3 247 A and 3 273 A, which are readily visible in the spectrograms obtained with an ultra-violet sensitive spectrograph (as shown in Plate 5), are not observed in spectrographs with glass optical components, and this may explain the reported non-existence of copper in the spectra of some workers employing a similar arc-heated, low-density wind tunnel[3]. Tungsten is a difficult element to detect, as although many lines are expected in the near ultra-violet and visible regions, all are faint and it is not advisable to assume that the element is absent. A few lines have been detected on well-exposed spectrograms, notably the sensitive line at 4 008 A.

The presence of metallic atoms in hot gas, especially the easily ionized copper, is of great significance when assessing the physical properties of the gas. At low enthalpy levels of the argon flow, where the argon ionization fraction is negligible, the majority of electrons present in the jet are undoubtedly derived from the copper contaminant.

7.4 The argon multiplets

A prominent feature of the visible argon spectrum is the division into sets of lines, which gives the appearance of a divided spectrum - a group in the blue region and another in the red. The brighter lines in the red region are known to possess some degree of self-absorption[25,26], and require careful determination of this effect before the relative intensities of the lines can be measured. Measurement of this effect will be attempted, but this group of lines does not feature in the present work. The blue lines, however, do not possess this effect to any appreciable degree and are always prominent in the spectra taken at all the ranges of power input available. The lines possessing known transition probabilities are listed in Appendix II, and the blue lines are indicated in a typical spectrogram (Plate 3).

7.5 Ionized argon

Even at high power inputs the lines originating from ionized atoms of argon are invariably extremely faint, although the neutral Ar I lines have sometimes been much overexposed. Some of the Ar II lines possess known transition probabilities (see Appendix II), and, if detected, a similar procedure may be adopted to determine an excitation temperature for the ionized atoms. (Such a temperature must be distinguished from the 'ionization temperature', see Sections 2 and 9.4). Other properties may be derived from the intensities of these lines e.g., the degree of ionization in the gas (by comparing the concentrations of Ar I and Ar II sources), and the ionization temperature at which these concentrations exist.

The Ar II spectrum becomes as important as the Ar I groups when the gas stream is stagnated in front of a blunt body placed in the jet, since here the temperature rises to the value attained in the plenum chamber (Fig. 10) before the gas is expanded in the convergent-divergent nozzle.

Spectra of the arc itself have been recorded with the light reflected from a polished copper surface introduced into the gas stream at the nozzle exit.

Such/

---

*The most readily detectable lines of a given spectrum are sometimes referred to as 'sensitive lines'.

Such spectra show the Ar II lines to be equal in intensity to the Ar I spectrum. Light from the arc, which has been observed in this manner, has of course penetrated a very long path through the cooler gas in the region between the nozzle exit and the electrodes (see Fig. 10). Generally, however, the light which was used to obtain the spectra for the temperature determinations was emitted from a small region in the jet, 10 mm from the nozzle exit, approximately 4 mm in height and 4 mm wide. The diameter of the jet is 20 mm.

8. The Derivation of Theoretical Temperatures from Aero-Thermodynamic Principles

Provided that some assumptions are accepted, estimates can be produced by different theoretical approaches for the temperature of a monatomic gas at the exit of the wind-tunnel nozzle. Extensive data concerning the operating conditions are required for these evaluations (e.g., power input to the electrodes, heat losses and efficiency, plenum chamber conditions, external pressure, nozzle characteristics, mass flow rate of the gas, etc.).

8.1 Concerning equilibrium

Three alternative hypotheses concerning the gas flowing through the system must be considered. They assume respectively the presence of either 'equilibrium flow' or 'frozen flow' conditions or else the 'lack of thermal equilibrium' (in aerodynamics the latter corresponds to 'non-equilibrium flow'). Frozen flow is an extreme case of non-equilibrium flow in which relaxation effects are negligible, i.e., relaxation times tend to infinity.

8.1.1 Equilibrium flow

In these problems the equilibrium flow treatment is usually applied to an ionized perfect gas, and properties such as the specific heats c_p and c_v, the degree of ionization, etc., are expected to change as the gas passes from the plenum chamber through the convergent-divergent nozzle.

The Mollier diagram for argon[27] was used to obtain estimates of both the equilibrium temperature and the ionization fraction at the nozzle exit for four sets of conditions, as set out in Table 3, Section 10.6. The arc heater efficiency was taken as 0·35, the plenum chamber temperature and ionization fraction were determined from the Mollier diagram, and the process extrapolated isentropically to the nozzle exit.

8.1.2 Frozen flow

Under frozen flow conditions the ratio of the specific heats, the sound velocity and the degree of ionization α_o are assumed to remain constant as the gas flows through the convergent-divergent nozzle. The arc heater efficiency is again taken as 35%.

If T_o is the gas temperature in the plenum chamber, and T is the nozzle exit temperature, then

$$T_o/T = 1 + \{(\gamma_o - 1)\ (Ma)^2\}/2 \qquad \ldots(8.1)$$

where, for frozen flow, γ_o is the ratio of the specific heats c_p/c_v (for argon $\gamma_o = 1{\cdot}67$),

(Ma) is the 'frozen Mach number' for the emergent stream given by u/a_o, u being the stream velocity and a_o the 'frozen speed of sound' in that stream.

See Section 10.6 for the results of this method.

8.1.3 Non-equilibrium flow

Application of the concept of non-equilibrium flow will infer that the physical properties of the gas flowing through the nozzle lie between the two extremes indicated by the above approaches.

8.1.4 Local thermodynamic equilibrium

Although either frozen flow or non-equilibrium flow hypotheses might be considered to be the required practical approach, they do not necessarily rule out the possibility of the application of the concept of 'local thermodynamic equilibrium'. In this case, the term 'local thermodynamic equilibrium' may be taken to imply that the translation energy and excitation energy modes of the atoms can be considered to be in equilibrium together, even if the gas, as a whole, is not. This concept is discussed in Refs. 8 and 28.

9. The Dissipation of Energy in the Plasma Jet

9.1 The energy balance

The energy input to the electrodes is directed into six sinks:-

(a) Heat loss to the electrodes, plenum chamber and nozzle combination. The quantity of energy so dissipated is determined by measuring the temperature rise of the cooling water to the head, and an efficiency η is defined as

$$\eta = 1 - \frac{\text{power input to cooling water}}{\text{power input to electrodes}}.$$

The value of η varies from one run to the next and does not appear to be a function of mass flow or of power input. Its value is normally 0·30 to 0·35 (Ref. 1). It will be noted that this figure applies to the entire head assembly, and does not necessarily indicate the fraction of the input energy which reaches the plenum chamber.

(b) Energy dissipated in the form of random kinetic energy of the atoms, ions and electrons present, given by $(5/2)NkT$, where

N = number of particles under consideration,

k = Boltzmann's constant

and T = translation temperature of that class of particle.

(c) Energy dissipated as directed kinetic energy of the particles along the axis of the gas jet, given by $(1/2)mu^2$ where

m = total mass of particles under consideration

and u = mean drift velocity along jet axis.

For a homogeneous jet, the mean drift velocity u is the aerodynamic free-stream velocity.

(d)/

(d) Energy absorbed by ionization of the working fluid, given by $\alpha N\chi$ where

α is the fraction of atoms ionized,

N is the total number of atoms under consideration,

and χ is the first ionization potential of working gas.

(e) Energy emitted in the form of electromagnetic radiation. This form of energy dissipation is generally regarded as being negligible in such energy balance equations, although it is difficult to find references to actual physical determinations of the magnitude of the effect in argon at elevated temperatures. Calorimetric total radiant flux measurements by Cann and Ducati[29] give a maximum of 5% of the total input energy being emitted as radiation. An earlier theoretical check[30] on argon at 16 000°K revealed an extra specific enthalpy due to excited atomic states of only 1·7% of the total enthalpy, at similar densities.

(f) Energy absorbed in the liberation and ionization of electrode material, given by $\beta N(\phi + \alpha_{con}\,\chi_{con})$ where

N = total number of particles of working gas present,

β = fractional contamination,

ϕ = surface work function of contaminant,

α_{con} = fractional ionization of contaminant,

χ_{con} = first ionization potential of contaminant.

Assuming a maximum copper contamination of 0·1% (which corresponds to an electrode erosion rate of about 4 g/hour), and that all of the copper is ionized, the energy absorbed by the contaminant dE_{con} becomes

$$dE_{con} = 0{\cdot}001\ (\dot{m}\,N_o/M)\ (\phi_{Cu} + \chi_{Cu})$$

where $(\dot{m}\,N_o/M)$ is the argon mass flow rate in atoms per second,

$\dot{m}$ is the mass flow rate in grammes per second,

N_o is Avogadro's number

and M is the argon molecular weight.

Now $\phi_{Cu} = 3{\cdot}29$ eV and $\chi_{Cu} = 7{\cdot}72$ eV, and therefore it can be seen that

$$(\phi_{Cu} + \chi_{Cu}) < \chi_{Ar}$$

and, as the kinetic energies of the copper atoms can only total about 0·2% those of the argon atoms, the amount of work expended upon the contaminant is negligible at appreciable levels of argon ionization. At low values of α_{Ar} however, the contaminant must make a significant contribution to the electron population, such electrons absorbing a considerable quantity of the input energy, gaining a high T_e at low electron densities, and thus restricting the gas temperature.

9.2 Energy balance at low power levels

At low power inputs, where the free-stream ionization $\alpha_\infty \simeq 0$, the input energy dissipates entirely as random and directed kinetic energies of the atoms (neglecting radiation) according to the relation

$$\eta E = \tfrac{5}{2} k T'_a (\dot{m} N_o/M) + \tfrac{1}{2} \dot{m} u_\infty^2 \qquad \ldots(9.1)$$

where E = head power input,

$\dot{m}$ = gas mass flow rate, g s^{-1},

N_o = Avogrado's number,

M = gas molecular weight

and T'_a = measured excitation temperature at low enthalpy.

Rearranging to solve for u_∞, the free-stream velocity at low enthalpy, we have

$$u_\infty^2 = \frac{2M\eta E - 5kT'_a \dot{m} N_o}{M\dot{m}}. \qquad \ldots(9.2)$$

9.3 Energy balance at elevated power levels

As the power input is increased from the low enthalpy conditions discussed above to such a level as to produce appreciable ionization, accompanied by a corresponding increase in excitation temperature dT, three principal sinks are available to dissipate the extra energy dE.

(a) Energy employed in ionization.

(b) Increased random kinetic energy, the temperature having risen to $T_a = (T'_a + dT)$, and the total number of particles having increased by a factor $(1 + \alpha)$, where α is the ionization fraction.

(c) Increased directed kinetic energy, again having regard to the increased number of particles and defining a new atom (and ion) free-stream velocity u_a and an electron velocity u_e.

Denoting these energy quantities respectively dE_i, dE_r and dE_d, and neglecting increased radiation and contaminant losses, we have the relation

$$dE = dE_i + dE_r + dE_d \qquad \ldots(9.3)$$

where dE is the extra energy input to the gas,

$$dE_i = \alpha(\dot{m} N_o/M)\chi \qquad \ldots(9.4)$$

$$dE_r = \tfrac{5}{2} k (\dot{m} N_o/M) (dT + \alpha T_e) \qquad \ldots(9.5)$$

and

$$dE_d = \tfrac{1}{2} \dot{m} u_a^2 - \tfrac{1}{2} \dot{m} u_\infty^2 + \tfrac{1}{2} m_e u_e^2 \alpha(\dot{m} N_o/M). \qquad \ldots(9.6)$$

In/

In order that equation (9.3) may balance upon substitution of the expressions (9.4), (9.5), (9.6), it is necessary that appropriate values be assigned to the parameters α, T_e, u_a and u_e.

9.4 Degree of ionization

It may be shown that equation (4.5),

$$I = (K'A\, h\nu N\, g/U) \exp(-E/kT),$$

is applicable to any excited atom or excited ion, for an optically thin source. An excellent derivation of this relation, including absorption terms, is given by Wilkerson[28], who shows that the constant K' includes a term for the length of the emitting source along the direction of emission. Thus the results may well be influenced by dissimilar radial profiles of the temperature and number density distribution of atoms and ions across the jet.

Employing subscript 'a' to indicate atoms and 'i' to indicate ions, we may thus derive:

$$\frac{N_i}{N_a} = \frac{(gA)_a\, \lambda_i\, I_i\, U_i(T)}{(gA)_i\, \lambda_a\, I_a\, U_a(T)} \cdot \exp\left(\frac{E_i - E_a}{kT}\right). \qquad \ldots(9.7)$$

Here, the values of gA, λ and E are given in Appendix II; the values of partition functions U(T) for neutral and ionized argon are given by Pike[31]; the value of T, assumed to be the same for Ar I and Ar II, is optimised from Figs. 12 or 13; and the intensity ratio I_i/I_a is determined by the previously described photographic methods.

The ionization fraction α is given by the relation

$$\alpha = N_i/(N_i + N_a).$$

Under conditions of thermal equilibrium, the Saha equation may be applied. This can be written in the form:-

$$\frac{n_i n_e}{n_a} = \frac{2U_i(T)}{U_a(T)} \cdot \frac{(2\pi\, m_e\, kT)^{3/2}}{h^3} \cdot \exp\left(-\frac{\chi_o}{kT}\right) \qquad \ldots(9.8)$$

where n = particle number density,

m_e = electronic mass,

h = Planck's constant,

χ_o = first ionization potential

and T is defined as the ionization temperature.

Under equilibrium conditions in a homogeneous gas, with a negligible electron contribution from impurities, $n_i = n_e$, and the ionization temperature

is/

is equal to the excitation and translation temperatures. Variations in electron density affect the validity of equation (9.7) (Refs. 9, 32). Equation (9.8) may be solved upon substitution of the value of n_i/n_a determined by equation (9.7) either for n_e, by assuming the equality of the ionization and excitation temperatures, or for T, by setting $n_i = n_e$ and assuming a value of α.

The attempt to measure the value of α using equation (9.7) was not wholly successful, as discussed in Section 10.5. Hence in the calculations which follow, values of α of 0·15 and 0·20 are chosen, based upon aerodynamic data given in Section 10.6.

9.5 Electron temperature

The electron temperature T_e will differ from the gas temperature T_a, except under conditions of absolute thermal equilibrium, this being due to the fact that the two classes of particles settle into individual Maxwell-Boltzmann velocity functions having differing distribution parameters. This occurs because, owing to their considerable mass difference, the atoms and electrons are effectively isolated energetically compared to the readiness with which they can exchange energy inter se. The original full treatment of non-equilibrium ionization theory by Petschek and Byron[33] balances the energy lost by the electron gas (this being due to inelastic collisions, causing atomic excitation or ionization), against the energy gained by elastic collisions. As this treatment, however, ignores recombination effects, it inevitably results in a derivation that gives $T_a > T_e$ under all conditions.

A full study by Bray and Wilson[34,35], applied to conditions of prevalent recombination, as in a supersonic nozzle, shows that in a recombination region $T_e > T_a$, and from their data a ratio T_e/T_a may be interpolated for the free-stream conditions. Using $\alpha = 0{\cdot}15$ to $0{\cdot}20$, a value of T_e/T_a of 1·05 to 1·25 is obtained.

It is interesting to note that Brundin, Talbot and Sherman[3] measured an electron temperature of the order 2×10^4 °K compared to a free-stream gas temperature of around 400°K, employing Langmuir probe techniques. The ionization fraction was, however, only 0·006. Their Mach 6 tunnel operated at 6 kW input, and their mass flow and pressure parameters were similar to those employed in our facility.

9.6 Particle drift velocities

Unless very large electric fields are to be set up within the plasma by electron diffusion, it is obvious that the condition $u_a \simeq u_e$ must be satisfied. Furthermore, if such fields are set up, they will clearly tend to negate the electron diffusion[36].

Calculations of the free-stream Mach number of the facility, based upon the ratio of the pitot pressure, measured by a probe placed in the stream, to the nozzle exit pressure, indicate a linear increase of Mach number from 2·8 to 3·0 over the power input range 10 to 50 kW. Comparison with the data of Table 3 indicates that the Mach number appears to increase linearly with the measured excitation temperature.

The initial particle velocity at low enthalpy, u_∞, has been determined by equation (9.2). If the frozen Mach number is held constant as the enthalpy increases, the frozen sound velocity being given by

$$a_o^2 = \gamma_o(1 + \alpha)T$$

where the ionization fraction $\alpha = \alpha_o$ = constant independent of enthalpy, then the atom velocity at elevated power inputs becomes:-

$$u_a^2 = u_\infty^2 \frac{T_a}{T'_a}(1 + \alpha) \qquad \ldots(9.9)$$

where T_a is the measured excitation temperature at that enthalpy.

If the frozen Mach number is considered as increasing, from the measured values of (Ma) = 2·8 at low enthalpy to 3·0 at high enthalpy, then, under these conditions, equation (9.9) becomes

$$u_a^2 = 1{\cdot}15\, u_\infty^2 \frac{T_a}{T'_a}(1 + \alpha). \qquad \ldots(9.10)$$

It will be noted that the ratio u_e/u_a must be of the order 300 before the directed kinetic energy of the electrons becomes comparable to that of the heavy particles.

9.7 Assumptions affecting the energy balance

These assumptions are:-

(a) That the efficiency η is constant at 0·35, and that this figure gives the fraction of the electrode input energy reaching the plenum chamber.

(b) That the random translational temperature of the gas, of which the random kinetic energy is a function, is equal to the measured excitation temperature.

(c) That at the low enthalpy values, $\alpha = 0$.

(d) That the radial distributions of temperature, particle density, ionization fraction and free-stream velocity are uniform, whereas there is reason to believe that they are in fact quite diverse functions having differing mean values.

(e) That the energy emitted in the form of electromagnetic radiation is negligible.

(f) That energy absorbed in liberation and ionization of electrode material is negligible.

10. Results

10.1 Excitation temperatures

The results of this investigation are presented in the form of two graphs, each for different argon mass flow rates, which are plots of the measured

excitation/

excitation temperature T in degrees Kelvin, against power input to the electrodes in kilowatts (Figs. 12 and 13). The plots show a near linear increase of T with power input, from around 4000°K at 15 kW to around 4800°K at 60 kW, for both of the mass flow rates considered. The general scatter of the points appears to be around ±5%, and the curves may well fall off somewhat at the low enthalpy extremes of the abscissae.

10.2 Associated errors

10.2.1 Errors in the power input measurements

Errors in determining the power input arise in reading the plasma jet voltmeter and ammeter, and from the degree of fluctuation in these values during a lengthy exposure. Further the quantity of energy actually transferred to the gas varies with the operating efficiency, which varies slightly from one run to the next, as discussed in Ref. 1. In general, the random error in the abscissae of the appended graphs may be estimated as being of the order ±5%.

10.2.2 Errors portrayed in relative intensity plots

Errors in the temperature measurements are estimated by the degree of scatter of the experimental points from the "best straight line" through those points on the $\log (I\lambda/gA)$ versus E_n plots. A typical plot is included in this report (see Fig. 11). Twelve experimental points are identified by the wavelengths of the spectral lines to which they refer, and the straight line is that calculated by the method derived in Appendix III. The standard deviation of the points from the line is a function of the probable error in the gradient of the line, as indicated in that Appendix. This fractional error in gradient, which is equal to the fractional error in temperature, is likely to be ±5%.

10.2.3 Effect of changes in argon flow rate on results

The argon mass flow rate is known accurately to ±2%, but, as will be seen from a comparison of Figs. 12 and 13, this parameter does not have much effect upon the results, at the flow rates used in this experiment.

10.3 Tables

Tables 1 and 2 set out the measured values of temperature against electrode power input, and indicate additionally the value of ρ/ρ_o for the argon heated and expanded within the jet, where ρ_o is the density at s.t.p.

Table 1/

Table 1

Gas Flow Rate: 70·3 g min^{-1}, (0·155 lb min^{-1})
or 0·657 l s^{-1} at s.t.p.

Spectrum No.	Power Input kW	Excitation Temp. °K	Gas Density ρ/ρ_o
3 N 30 78	15·3	4 430	
1 N 50 70	16·8	4 270	
11 N 50 64	17·5	4 310	6×10^{-4}
5 N 50 42	18·6	4 170	
3 N 30 50	19·2	4 430	
3 N 30 36	23·7	4 500	
11 N 50 50	25·2	4 630	5×10^{-4}
10 N 50 64	25·7	4 570	
10 N 50 36	25·7	4 530	
3 N 30 22	28·6	4 200	
3 N 30 08	33·6	4 150	3×10^{-4}
13 N 50 36	34·0	4 400	
4 N 30 64	39·1	4 640	
14 N 50 78	41·4	4 510	
14 N 50 64	45·5	4 470	
4 N 30 50	48·3	4 460	
14 N 50 36	52·2	4 830	
4 N 30 36	53·1	4 780	
14 N 50 22	56·3	4 670	1×10^{-4}

ρ_o is the density of argon at s.t.p.

Table 2/

Table 2

Gas Flow Rate: 99·0 g min^{-1}, (0·218 lb min^{-1})
or 0·925 l s^{-1} at s.t.p.

Spectrum No.	Power Input kW	Excitation Temp. °K	Gas Density ρ/ρ_o
12 N 50 36	27·0	4 270	
5 N 30 64	30·6	4 290	$7{\cdot}5 \times 10^{-4}$
5 N 50 28	31·8	4 230	
9 N 50 12	32·3	4 370	
12 N 50 22	33·3	4 270	
13 N 50 64	37·4	4 380	8×10^{-4}
5 N 30 50	40·8	4 540	
5 N 30 36	47·8	4 360	
14 N 50 50	48·8	4 420	
5 N 30 22	59·9	4 600	$8{\cdot}5 \times 10^{-4}$
14 N 50 08	61·1	4 580	
5 N 30 08	63·7	4 660	
13 N 50 08	65·3	4 370	1×10^{-3}

10.4 The distribution of experimental points in the relative intensity plots - resulting transition probabilities

While the apparent errors in the relative intensity plots discussed in Section 10.2.2 appear to be rather large, in fact the various plots for the spectrograms evaluated show a consistent pattern of the points, and indicate individual systematic errors for those points. Since large errors are known to exist in the values of some of the transition probabilities given by various workers (10% to 25%), it is reasonable to assume that those points which appear in extraordinary positions relative to the majority of points (and do so consistently, in spite of significant changes in the operating conditions of the arc), could be adjusted to agree with the other points. This was attempted for those points which were obviously incorrect, and subsequent plots were apparently successful when the corresponding new transition probabilities were employed.

Those values actually employed in the calculations are indicated by an asterisk in the transition data table of Appendix II.

10.5/

10.5 Attempted measurement of the ionization fraction

An attempt was made to determine the ionization fraction α by measuring the intensity of the 4348 A ArII line, which is, in general, the strongest line in the ArII spectrum for which the transition probability can be quoted, and comparing it to the adjacent 4345 A ArI line. The theory is set out in Section 9.4.

It was found that, whilst all the other relevant parameters were well known, it was not possible to determine the intensity ratio I_i/I_a to any accuracy. The exposure time necessary to obtain the ArII line at 4348 A was greater than 20 minutes, as compared to a typical figure of 10 seconds for an ArI spectrogram. As a result of this extended exposure the plate was heavily fogged owing to nitrogen band and continuum radiation. The densitometer trace of the ArII line just showing above the background was open to rather liberal interpretation, and a knowledge of the reciprocity characteristic of the plate was necessary, as direct ArI - ArII comparisons were not possible. Employing equation (9.7), and using data supplied by Messrs. Ilford Ltd.[37] (see Section 13.3 (c)) to assist in the elimination of the reciprocity effect, a value of α of 0·40 was obtained. Making the generous allowance of a possible order of magnitude error in the ratio I_i/I_a, the value of α must be at the very least 0·07. The flow parameters were $\dot{m} = 1$ g s^{-1} and power input = 50 kW.

It seems doubtful that any subtle improvement in the spectrographic technique can fully overcome the inherent difficulties, although an effort is being made to reduce the quantity of nitrogen leaking into the working section.

The Saha equation (Section 9.4, equation (9.8)) was solved for n_e, the electron density, assuming $T_{excitation} = T_{ionization}$, and a value of 10^{5} electrons cm^{-3} resulted, at 50 kW input and $\dot{m} = 1$ g s^{-1}. This compares to a total particle density of the order 10^{15} cm^{-3}. An error of an order of magnitude in the measured intensity ratio I_i/I_a gives rise to the same error in n_e.

A solution was also obtained for T assuming a value of $\alpha = 0{\cdot}20$ and putting $n_i = n_e$. Under the same equilibrium conditions as indicated above, a value of $T = 8400 \pm 500$°K resulted, the error allowing for an order of magnitude error in I_i/I_a.

10.6 Comparison with aerodynamic data (see also Section 8)

Table 3 sets out a comparison between the spectroscopically determined excitation temperatures and the aerodynamically determined exit temperatures for four sets of conditions. The excitation temperatures, which are measured about 10 mm downstream of the nozzle exit, have been optimised from Figs. 12 and 13. Throughout these calculations the head efficiency η has been taken as 0·35.

Table 3/

Table 3

	Run No.			
	1	2	3	4
Mass flow, g s^{-1}	1·17	1·17	1·65	1·65
Head input, kW	18·6	52·2	17·8	61·1
Input to gas, kW	6·51	18·3	6·23	21·4
Measured excitation temperature °K	4345	4715	4130	4490
T_{exit} (equilibrium) °K	3500	9400	2700	8900
T_{exit} (frozen) °K	2480	3230	1880	3200
T_o (plenum) °K	9200	12000	7000	11900
α_o (plenum)	0·02	0·21	0·001	0·16

10.7 Energy balance calculations

10.7.1 Free-stream velocity at low enthalpy

The free-stream velocity at reduced enthalpy levels, u_o, was determined from the data of Table 3 employing equation (9.2):

	Run No.	
	1	3
u_o cm s^{-1}	$2·63 \times 10^5$	$1·80 \times 10^5$
(u_o ft s^{-1}	$8·63 \times 10^3$	$5·92 \times 10^3$)

10.7.2 Energy balance calculations at elevated enthalpies

Under the operating conditions set out in Table 3, assuming initially $\alpha = 0·15$, $T_a = T_e$ and u_a is given by equation (9.9), the components of equation (9.3), i.e.,

$$\Sigma dE = dE_i + dE_r + dE_d$$ become:

Run Nos./

	Run Nos.	
	1 & 2	3 & 4
dE	$1{\cdot}18 \times 10^4$	$1{\cdot}52 \times 10^4$
dE_i	$6{\cdot}66 \times 10^3$	$9{\cdot}38 \times 10^3$
dE_r	$6{\cdot}52 \times 10^2$	$8{\cdot}83 \times 10^2$
dE_d	$9{\cdot}50 \times 10^2$	$6{\cdot}79 \times 10^2$
ΣdE	$8{\cdot}26 \times 10^3$	$10{\cdot}94 \times 10^3$
$\Sigma dE/dE$	70%	72%

(All energy rates are expressed in watts)

If now a value $T_e = 1{\cdot}1\ T_a$ at $\alpha = 0{\cdot}15$ is adopted, and the value of u_a is that given by equation (9.10), the results obtained are:

	Run Nos.	
	1 & 2	3 & 4
dE	$1{\cdot}18 \times 10^4$	$1{\cdot}52 \times 10^4$
dE_i	$6{\cdot}66 \times 10^3$	$9{\cdot}38 \times 10^3$
dE_r	$6{\cdot}98 \times 10^2$	$9{\cdot}44 \times 10^2$
dE_d	$1{\cdot}75 \times 10^3$	$1{\cdot}18 \times 10^3$
ΣdE	$9{\cdot}11 \times 10^3$	$1{\cdot}15 \times 10^4$
$\Sigma dE/dE$	77%	76%

Calculations based upon a value of $\alpha = 0{\cdot}02$, with $T_e = 1{\cdot}15\ T_a$ and u_a given by equation (9.10), give values:

	Run Nos.	
	1 & 2	3 & 4
dE	$1{\cdot}18 \times 10^4$	$1{\cdot}52 \times 10^4$
dE_i	$8{\cdot}88 \times 10^3$	$12{\cdot}5 \times 10^3$
dE_r	$8{\cdot}84 \times 10^2$	$11{\cdot}9 \times 10^2$
dE_d	$1{\cdot}76 \times 10^3$	$1{\cdot}34 \times 10^3$
ΣdE	$1{\cdot}15 \times 10^4$	$1{\cdot}50 \times 10^4$
$\Sigma dE/dE$	97%	99%

11./

11. Conclusions

Densitometric measurements from spectrograms still appear to be useful as a technique for comparing the intensities of a large number of close spectral lines when the observation exposure time is limited to a few seconds. Much time is saved if a high resolution spectrograph is employed with a wide slit. The γ factor for deriving intensities must be determined from individual spectral lines and not from standard tungsten lamp spectra.

Radiation from argon ions has been detected in the free stream only in cases where very extended exposure periods have been employed, although ArII lines are readily observed in the arc and behind shock fronts. Copper and tungsten are observed in the free stream, and hydrogen, oxygen, nitrogen, NH and OH are observed in the surrounding low pressure atmosphere. The predominance of the second positive band system in this nitrogen spectrum appears to confirm the presence of metastable states of argon.

It is considered that the excitation temperature is a close indication of the translation temperature, provided that the concentration of free electrons is low. However, it has been pointed out[66] that even for low electron densities, electron-atom collision cross-sections can be large and that there is a distinct possibility of the higher atomic quantum levels equilibrating to the electron temperature rather than to the gas temperature. This has been demonstrated experimentally by Hinnov and Hirschberg[67], and theoretically by Makin and Keck[68] and by Byron et al[69], amongst others. They show that there exists a "bottleneck" quantum level n^* owing to the high probability of collisional, rather than radiative, de-excitation at the levels designated by large quantum numbers, whereas these levels are, according to the Maxwell-Boltzmann statistics, sparsely populated. Accordingly, de-exciting transitions taking place from levels above n^* are three-body collisional processes and as such must be considerably dependent upon the energy of the free electrons. As there is a possibility of the electron temperature within our plasma being somewhat higher than the gas temperature, and as the value of n^* has not been calculated, there would seem to be some finite possibility that the measured values of excitation temperature are not identical to the translational temperature.

The excitation temperatures measured in the free stream of the arc-heated argon wind tunnel have values lying between the equilibrium flow temperatures and the frozen flow temperatures, with, in general, a bias towards the latter (cf. Table 3, Section 10.6).

An attempt to measure the free-stream ionization fraction α, by comparison of the intensities of the 4348 A ArII and 4345 A ArI lines, indicated a value even higher than that corresponding to perfect frozen conditions. Considering the magnitude of the possible random errors in this calculation a free-stream ionization of at least 8 - 15% is indicated.

A successful energy balance resulted assuming a free stream α of 0·15 to 0·20. Should the free-stream ionization prove to be substantially less than this figure, i.e., the flow being nearer to equilibrium and further from frozen than appears at present, then it may prove difficult to explain what is happening to a large proportion of the input energy.

Solution of the Saha equation for n_e, assuming equality of the excitation and ionization temperatures, and employing the ratio n_i/n_a as

determined/

determined from the intensity ratio of the 4345 - 4348 A lines, resulted in an n_e of 10^5 electrons cm^{-3}. This figure corresponds to an $\alpha \sim 10^{-10}$, whereas the measured α based upon the value of n_i/n_a was 0·40. The possible error in the intensity ratio cannot explain this discrepancy. However, such a result, at this stage of the investigation, is not particularly surprising, for an explanation could be that the flow condition is so far from equilibrium as to render the Saha equation meaningless, i.e., that the excitation and ionization temperatures differ considerably* (the parameter T in the Saha equation must be about twice the measured excitation temperature to give an α of 0·20).

The consistent pattern of points on the log $(I\lambda/gA)$ versus E graphs would appear to indicate that local thermodynamic equilibrium exists between the excitation and translation modes of the atoms of the gas at the nozzle exit.

The present data of argon transition probabilities is now sufficiently expanded to permit consistent results to be obtained. The probabilities for some lines appear to need some adjustment, since such lines produce consistently deflected points on the log $(I\lambda/gA)$ versus E plots.

12. Acknowledgements

We are indebted to Prof. A. G. Gaydon of the Chemical Engineering Department and Dr. W. R. S. Garton of the Physics Department, Imperial College, for the generous loan of instruments and for much practical advice. Thanks are also due to L. A. King of the Electrical Research Association for a very profitable discussion on the techniques and problems of spectrometric measurements, and above all, for directing our attention to the relevant literature on the subject.

For a most helpful discussion on the merits of various types of spectrograph suitable for this work, we thank Dr. Anne Thorne and Dr. R. Learner of the Physics Department, Imperial College and Dr. K. C. Lapworth of the National Physical Laboratory.

It would be an injustice not to include a tribute to W. E. Gericke, formerly of Kiel University, because, without his obviously diligent determinations of transition probabilities, we realise that no significant results could yet have been obtained.

Acknowledgements are also expressed to J. L. Stollery of the Aeronautics Department, for initiating this research programme and submitting with grace to our persistent demands for yet more apparatus. We are also grateful for his counsel and thorough editing of this report. Nevertheless, the authors take responsibility for any opinions expressed within.

References/

* Dewan[38], shows that where steady-state conditions prevail, but the particle energy distribution is not exactly Maxwellian, or where radiation leaves the system without absorption, significant numerical deviations from the Saha relation are to be expected.

References

No.	Author(s)	Title, etc.
1	J. K. Harvey and P. G. Simpkins	A description of the Imperial College arc-heated wind tunnel. J.R.Ae.Soc., 66, 637 (1962).
2	---	British Standard 1991. Letter symbols, signs and abbreviations. British Standards Institution, London, W.1.
3	C. L. Brundin, L. Talbot and F. S. Sherman	Flow studies in an arc-heated, low-density supersonic wind tunnel. University of California, Institute of Engineering Research, Tech. Rep. No.HE-150-181 (1960).
4	L. E. Brewer and W. K. McGregor	Excitation of nitrogen by metastable argon atoms. Phys. Fluids, 5, 1485 (1962).
5	L. R. Ryan, H. J. Babrov and R. H. Tourin	Infrared spectra and temperatures of plasma jets. II. Spectrometric and spectroradiometric measurements of plasma jet temperature distributions. Warner & Swasey Co. Control Instrument Division, Downing Street, Flushing 54, NY. ARL Contract No.33(616)-8057
6	H. Edels	The determination of the temperatures of an electrical discharge in a gas. A résumé. British Electrical & Allied Industries Research Association Technical Report No. L/T 230 (1950).
7	H. K. Sen	Astrophysicists' concept of temperature. Paper 16 in Energy transfer in hot gases. NBS Circular 523 (1951).
8	W. Lochte-Holtgreven	Production and measurement of high temperatures. Reps. on Prog. in Phys. (1958).
9	H. R. Griem	Plasma spectroscopy. From Proc. 5th International Conf. on Ionization Phenomena in Gases, Munich (1961), Vol.II, p.1857, North Holland, Amsterdam.
10	C. F. Knopp, C. F. Gottschlich and A. B. Cambel	The spectroscopic measurement of temperature in transparent argon plasmas. J. Quant. Spectr. Rad. Trans. 2, 297 (1962).

11/

No.	Author(s)	Title, etc.
11	W. J. Pearce	Plasma-jet temperature measurement. From Optical Spectrometric Measurements of High Temperatures. Edited P. J. Dickerman, pp.125-169, University of Chicago Press (1961).
12	L. H. Aller	Astrophysics. Vol: The atmospheres of the sun and stars. Ronald Press Co., New York, Ch.4 (1953).
13	C. W. Allen	Astrophysical Quantities. Athlone Press, London (1955).
14	National Bureau of Standards (Compiled by C. E. Moore)	Atomic Energy Levels, Vol.I. NBS Circular 467 (1949).
15	American Society for Testing Materials	Methods for chemical analysis of metals. (1960).
16	L. A. King	Private discussion.
17	J. K. Harvey, P. G. Simpkins and B. D. Adcock	Instability of arc-columns. A.I.A.A.J. 1, 714, (1963).
18	G. R. Harrison, R. C. Lord and J. R. Loofbourow	Practical Spectroscopy. Prentice-Hall, N.J. (1948).
19	L. R. Doherty	The measurement of absolute spectral line intensities with the shock tube. Ph.D. Thesis, University of Michigan (1961).
20	E. W. H. Selwyn	Photography in Astronomy. Eastman Kodak NY (1950).
21	L. W. Strock	Photographic factors influencing the concentration-calibration curve in quantitative methods of spectrochemical analysis, II. Spectrochim. Acta. 1, 123 (1939).
22	J. C. de Vos	Physica, 20, 690 (1954).
23	W. G. Fastie	A small plane grating monochromator. J. Opt. Soc. Amer., 42, 641 (1952).
24	E. S. Barrekette and R. L. Christensen	Blazed diffraction gratings. Paper WD.13, Spring Meeting of Opt.Soc.Amer. (1963).

25/

No.	Author(s)	Title, etc.
25	H. N. Olsen	Measurement of argon transition probabilities using the thermal arc plasma as a radiation source. J.Q.S.R.T. 3, 59, (1963).
26	P. J. Dickerman and B. P. Alpiner	Spectral line shapes and transition probabilities for argon. J. Quant. Spectr. Rad. Trans. 2, 305 (1962).
27	F. Bosnjakovic et al	Mollier enthalpy-entropy charts for high-temperature plasmas. Thermodynamic and Transport Properties of Gases, Liquids and Solids. Am. Soc. of Mech. Eng., N.Y. (1959).
28	T. Wilkerson	The use of the shock tube as a spectroscopic source with an application to the measurement of gf-values for lines of neutral and singly ionized chromium. University of Michigan, Ph.D. Thesis (1961), and AFOSR 11 15.
29	G. L. Cann and A. C. Ducati	Energy content and ionization level in an argon gas jet heated by a high intensity arc. J.F.M. 4, 529 (1958).
30	E. Resler, S. Lin and A. Kantrowitz	The production of high temperature gases in shock tubes. J. Appl. Phys., 23, 1390 (1952).
31	G. W. F. Pike	Approximate calculations of the internal partition function of A, A^{+} and A^{++} in the temperature range 4 000°K to 50 000°K. NRC MT-46 (1961).
32	W. Finkelnburg and H. Maecker	Handbuch der Physik, 22, part II.
33	H. E. Petschek and S. Byron	Approach to equilibrium ionization behind strong shock waves in argon. Ann. Phys. N.Y. 1, 270 (1957).
34	K. N. C. Bray and J. A. Wilson	A preliminary study of ionic recombination of argon in wind tunnel nozzles. A.R.C. C.P.559, February, 1960.
35	K. N. C. Bray and J. A. Wilson	A preliminary study of ionic recombination of argon in wind tunnel nozzles. Part II. A.R.C. C.P.634, July, 1961.

36/

No.	Author(s)	Title, etc.
36	G. A. Bird	Diffusion effects in the expansion of an ionized gas. Commonwealth of Australia, Department of Supply. Australian Defence Scientific Service, Weapons Research Establishment Technical Note HSA 47, January, 1959. A.R.C.21 181. July, 1959.
37	Ilford Ltd. (Research Labs)	Private communication.
38	E. M. Dewan	Generalizations of the Saha equation. Phys. Fluids 4, 759, (1961).
39	---	Ilford Technical Information Book, Vol.I. Ilford Ltd., Ilford, Essex.
40	---	"Kodak" Scientific Plates. Kodak Data Booklet SE-3, Kodak Ltd., London.
41	H. Kaiser	The various procedures for evaluating spectra in quantitative spectrochemical analysis. Spectrochim. Acta 2, 1 (1941).
42	D. C. Cordingley, L. J. Lacey and P. J. Sandiford	Extended table of Seidel function for spectrographers. App. Spectr. 8, 92 (1954).
43	M. Honerjager-Sohm and H. Kaiser	Spectrochim. Acta 2, 396 (1944).
44	J. D. Smith	Application of nomographs to spectrographic analysis of grey and low-alloy cast irons. Hilger J. 7, 43 (1962).
45	A. Mayer and W. J. Price	Chemical and spectrographic analysis of magnesium and its alloys. Magnesium Elektron Ltd., Manchester (1954).
46	H. K. Hughes and R. W. Murphy	Emulsion calibration for quantitative spectroscopic analysis. J. Opt. Soc. Amer. 39, 501 (1949).
47	G. R. Harrison and P. A. Leighton	Homochromatic spectrophotometry of the extreme ultra-violet. J. Opt. Soc. Amer. 20, 313 (1930).
48	R. A. Sawyer	Experimental spectroscopy. Prentice-Hall N.Y. (1951).

49/

No.	Author(s)	Title, etc.
49	T. P. Schreiber et al	Spectrum line distortion caused by step filters. App. Spectr. 14, 57 (1960).
50	National Bureau of Standards (Compiled by B. M. Glennon and W. L. Wiese)	Bibliography of atomic transition probabilities. NBS Monograph 50 (1962).
51	National Bureau of Standards (Compiled by C. H. Corliss and W. R. Bozmann)	Experimental transition probabilities for spectral lines of seventy elements. NBS Monograph 53 (1962).
52	G. R. Harrison	M.I.T. wavelength tables. Wiley, New York. (1939).
53	H. W. Drawin	Z. Physik 146, 295 (1956).
54	W. E. Gericke	Messung der Übergangswahrscheinlichkeit von AI-linien. Z. Astrophysik 53, 68 (1961).
55	H. N. Olsen	Temperature measurements in high current arc plasmas. Bull. Amer. Phys. Soc.(2), 4, 262 (1959).
56	H. N. Olsen	Private communication to Doherty (Ref. 14).
57	R. H. Garstang	M.N. Roy. Astron. Soc. 114, 118 (1954).
58	H. N. Olsen	Determination of properties of an optically thin argon plasma. Paper 60 in Temperature; its measurement and control in science and industry, Vol.3, Part I. Editors, C. M. Herzfeld and F. G. Brickwedde. Reinhold N.Y. (1962).
59	National Bureau of Standards (Compiled by C. E. Moore)	A multiplet table of astrophysical interest. NBS TN 36 (1945).
60	R. A. Buckingham	Numerical Methods. Pitman, London (1957 and 1962).
61	A. Pery-Thorne and J. E. Chamberlain	Transition probabilities in the spectra of neutral neon, argon and krypton. Proc. Phys. Soc. 82, 133 (1963).
62	L. P. Razumovskaya	Spectroscopic study of high-frequency discharges in argon. Optics & Spectr., 14, 98 (1963).
63	K. Schön	Ann. Phys. (Lpz.), 28, 649 (1937).

64/

No.	Author(s)	Title, etc.
64	J. Yarwood	(For basic theory of Atomic Spectra) Electricity, Magnetism and Atomic Physics. Vol.2: Atomic Physics, Chapters 4 and 5. University Tutorial Press (1958).
65	C. M. Herzfeld (Editor-in-Chief)	Temperature; its measurement and control in science and industry, Vol.III (1962).
	F. G. Brickwedde (Editor)	Part I: Basic concepts, standards and methods.
	A. I. Dahl (Editor)	Part II: Applied methods and instruments. Reinhold, N.Y.
66	K. N. C. Bray	Private communication.
67	E. Hinnov and J. G. Hirschberg	Electron-ion recombination in dense plasmas. Phys. Rev. 125, 795, (1962).
68	B. Makin and J. C. Keck	Variational theory of three-body electron-ion recombination rates. Phys. Rev. Lett. 11, 281, (1963).
69	S. Byron, R. C. Stabler and P. I. Bortz	Electron-ion recombination by collisional and radiative processes. Phys. Rev. Lett 8, 376, (1962).

APPENDIX I/

APPENDIX I

Photographic Emulsions and Calibration Techniques*

A.1 Emulsion Characteristics and Plate Selection

The following points are among those which must be taken into consideration when selecting an emulsion for a particular spectrographic purpose:

(1) Speed

Since the speeds of photographic plates vary very considerably, an emulsion must be selected which is compatible with the exposure time available. The latter will depend upon the photographic speed of the combined spectrograph and collecting optics, and must be of such a length as to integrate minor perturbations of the light source without being so long as to allow variation in the macroscopic properties of the source.

(2) Contrast

The degree of contrast required will depend upon the relative intensities of the lines to be studied within a given range. In general, it is more difficult to work with high contrast plates, as the judgement of exposure times is more critical, but they compensate for this by allowing increased accuracy when dealing with lines of closely similar intensities.

(3) Colour sensitivity

Four classes of photographic emulsions are readily available, encompassing the visible and adjacent regions:

(a) Unsensitized silver bromide emulsions, sensitive to the blue and ultra-violet only, from about 2 100 A - 5 000 A. A red safelight may generally be used when dealing with these "ordinary" emulsions.

(b) Orthochromatic, dyed to be sensitive up to the green.

(c) Panchromatic, dyed to be sensitive up to the red.

(d) Infra-red sensitive, useful up to about 9 000 A or further. It is necessary to store plates of this type in a refrigerator.

(4) Granularity and backing

Grain size (and hence speed), being in general reciprocal to contrast, is a factor which, combined with halation, limits the resolving power of the emulsion. Halation is an effect which manifests itself as the formation of a ring around the principal image, and is due to light scattering off the back face of the

glass/

---

* The reader is referred to Selwyn[20] for an excellent exposition of much of the matter contained in this Appendix.

glass plate. It can be minimized by backing the plate with a suitable soluble coating, which absorbs the would-be scattered light. Large grain size also tends to cause scattering from one grain to adjacent ones.

(5) Uniformity of colour response

The chemical composition of the emulsion determines the degree of uniformity or otherwise of the response of the plate to various wavelengths, which may be important if it is desired to assume constant colour sensitivity over a particular short range of wavelengths.

(6) Pressure sensitivity

Some plates are very sensitive to local contact of physical pressure, which must be avoided in order to prevent an effect similar to areas of fogging.

The properties of the plates manufactured by two principal concerns are well described in their technical data publications[39,40]

A.2 Characteristic Curves

The density function $D = -\log T$ is of only limited utility in that it is generally only linear for about one third of the total transmittance range, and other empirical relations exist which give a considerable extension to the linearity of the characteristic curve.

The Seidel function[41]

$$\Delta(T) = \log\left(\frac{1}{T} - 1\right)$$

is found to be eminently suitable for many emulsions, and is deemed in some cases to be capable of extending the linearity of the characteristic curve from $3\% < T < 97\%$. We have used this function entirely, and have found it satisfactory for at least $15\% < T < 85\%$ with the Ilford ordinary emulsions.

A table of values of $\Delta(t)$ at 0·2% intervals of T is given in Ref. 42.

The partially corrected Seidel function, which incorporates both the density and the Seidel functions, is represented by:

$$P_N(T) = \frac{D(T) + N \cdot \Delta(T)}{(1 + N)}$$

where N is a low number ~ 1. This function has been tabulated by Honerjäger-Sohm and Kaiser[43] for $N = 1$, and has been found to be very useful for extending the linearity of the characteristic curve for the panchromatic Kodak B.10 plate[44].

The relative utility of the $\Delta(T)$ and $P_1(T)$ functions is discussed by Mayer and Price[45] who find almost complete linearity using $P_1(T)$ for the

Kodak/

Kodak B.10, whilst for the Ilford N.50 they find the Seidel function gives better results. The best function for a given emulsion may be determined by plotting, for example, three extreme points for both the $\Delta(T)$ and $P_1(T)$ transformations, and by inspection finding those points which best fulfil the condition of collinearity.

A further function which is due to Hughes and Murphy, may be quoted[46]:

$$f(T) = \log \frac{T}{1 - T} - 0{\cdot}4 \exp (T).$$

This is seen to include $\Delta(T)$ as its principal term.

A.3 Intensity Calibration - Impression of Gradations*

Five principal methods are available for impressing upon the photographic emulsion the necessary gradations of the incident intensity, in known increments, in order to construct a characteristic curve.

(a) Rotating step filter. A logarithmically stepped disc is rotated in front of the spectrograph slit at the stigmatic position** such that a series of steps are formed on the plate, because some portions receive longer exposures than others. In general, an intermittent exposure does not produce the same density as the equivalent continuous exposure, and to overcome this difficulty the light beam must be interrupted some 200 to 1 000 times, thus demanding high rotational velocities[20].

(b) Evaporated metal stepped filter. A series of strips of metal such as rhodium or platinum, the individual strips having graded thicknesses, are evaporated on to a glass or quartz blank which is located, with the strips crossing the slit, at the stigmatic position of the spectrograph. This device clearly produces an effect similar to that of the rotating step filter.

(c) Taking several exposures of differing durations and ignoring reciprocity failure, which is allowable over certain ranges of extended exposures with some emulsions. The general validity of this method is, however, dubious, although it has the advantages of great simplicity and the fact that it is applicable to an astigmatic spectrograph. It is best only used as a checking procedure, unless steps have been taken to examine the reciprocity failure of the plate***.

(d)/

---

* The reader is referred to Harrison[18] for a concise summary of the available techniques.

** There is a point, usually upon the optical axis of an instrument, such that, if an object is placed at that point, an accurately rendered image of that object is reproduced at the position of the photographic plate. This point is termed the "stigmatic position".

*** In a paper concerning ultra-violet sensitization by fluoresceing oils, Harrison and Leighton[47] describe a method for determining the reciprocity characteristics of an emulsion, whilst reciprocity failure in general is discussed in detail in Refs. 18 and 20. Typical log I versus log It plots for several Kodak emulsions are given by Sawyer[48]. Messrs. Ilford Ltd., whilst stating that such data are too variable to merit publication, have supplied log (relative speed) versus log (exposure time) characteristics for the plates used[37]. These latter data have been employed in our calculations (Section 10.5).

(d) A specially constructed slit may be used with a stigmatic spectrograph, in which several aperture widths are simultaneously provided along the length of the slit.

(e) If the source can effectively be moved to various distances from the slit, the inverse square law can be applied to calibrate the densities arising from equal exposures corresponding to the different source positions. This technique is suitable for both stigmatic and astigmatic spectrographs.

The rotating step filter has the advantage over the evaporated step filter of possessing complete colour independence, whereas it is essential that the evaporated filter be density calibrated at frequent intervals, say 200 A, throughout the wavelength range of interest, as the relative transmittance of adjacent steps may vary very considerably over even a short range. The evaporated filter is, however, considerably easier to use, being a static device; whereas the rotating filter, which by its very nature is dynamically unbalanced, can be inconvenient in practice with its requirement for being rotated at about 1 200 rev/min. The evaporated filter can be fixed in place on the apparatus without need of maintenance and is more suitable for taking short exposures. A note by Schrieber[49] on possible line distortion which is attributable to step filters, describes how it may be necessary to tilt the plane of the filter a few degrees off normal to the incident light beam.

We have elected to employ a Hilger seven-step rhodium-on-quartz filter, calibrated at 200 A intervals over the range 2 800 - 8 000 A.

APPENDIX II/

APPENDIX II

Transition Probability Data

There has in the past been a marked lack of accurate transition probability data, these parameters having been previously of principal interest to astrophysicists. Over the past months, however, the situation has improved in view of increased interest in plasma physics and related fields, and an excellent bibliography has recently appeared[50] listing most of the presently known work on the determination of these parameters. Experimental measurements of transition probabilities have recently been published for some 70 solid elements[51] which will be of considerable use for the determination of contaminant or seeding levels at a later stage of this project.

The tables appended here, for ArI and ArII, are believed to include all available data to date. The arrangement of the tables for a transition from an upper state E_n to a lower state E_m is as follows:

Column (a) Wavelength, angstroms[52]

(b) $g_n = 2J_n + 1$

(c) $g_m = 2J_m + 1$

(d) E_n cm^{-1} (Ref. 14)

(e) E_n eV (conversion factor 8065·57) (See Section 4.5)

(f) Transition probability $A_{nm} \times 10^{-5}$ s^{-1}

(g) Estimated error dA/A %

(h) $\log_{10}(\lambda/gA)$

(i) $gA \cdot 10^{-5}$ s^{-1}

(j) An asterisk appearing in this column indicates the particular value of A which has been found to be most consistently reliable; in some cases the value so indicated will differ from that given in the references, but it will invariably be seen to be within the limits of the estimated error given therein (see Section 10.4). A double or treble asterisk in this column indicates that in addition to the values shown, relative gf values for these lines have recently been determined by Dickerman and Alpiner[26]. Lines marked ** are stated by these workers to demonstrate considerable self-absorption, whilst those marked *** apparently do not.

(k) References

Energy level diagrams for the spectral lines contained in the tables are set out in Figs. 15 and 16 for ArI and ArII respectively. The spectroscopic notation is that employed by Moore[59].

In/

In a recent paper, Razumovskaya[62] presents absolute f-values for some 17 red and infra-red and 7 blue-violet lines of neutral argon. These are based on a sum-rule computation of the f-number of λ8115, the other 23 values being determined by experimental comparison with this line. Her values in general lie considerably higher than those of other workers, notably in that her reference line λ8115 has an f-value some 2 or 3 times greater than that given by 5 other sources, and it is upon this value that the accuracy of the remaining readings depend. The oscillator strengths for the blue-violet lines given in this paper are two orders of magnitude greater than those obtained by Drawin[53], whose results are the only ones cited, other than a comparison with the early work of Schon[63].

Table/

Transition Probability Data, Argon ArI

(a)	(b)	(c)	(d)	(e)	(f)	(g)	(h)	(i)	(j)	(k)
3947·5046	5	5	118469·117	14·68	1·71	15	2·66435	8·55		53
3948·9785	3	5	118459·662	14·68			2·88638	5·13		
4045·966	5		118459·662	14·68	3·68	10	2·34222	18·4		53
4158·5906	5	5	117183·654	14·53	6·55	6	2·10377	32·75		25
					16·7	10	1·69726	83·5		53
					11·0	15	1·87858	55·0	*	54
4164·1794	3	5	117151·387	14·52	2·46	40	2·75147	7·38		53
					2·0	15	2·84138	6·0		54
					2·23		2·79410	6·69	*	
4181·8833	3	1	118459·662	14·68	4·16	15	2·52513	12·48		53
					3·8	15	2·56447	11·4		54
					4·58		2·48336	13·74	*	
4198·3174	1	3	117563·020	14·58	26	15	2·20811	26	*	54
4200·675	7	5	116942·815	14·50	7·6	15	1·89741	53·2	*	54
4251·1848	3	5	116660·054	14·46	0·79	15	3·25368	2·37		54
					0·85		3·22198	2·55	*	
4259·361	1	3	118870·981	14·73	24·6	9	2·23841	24·6		25
					39·7	15	2·03051	39·7		53
					36	15	2·07304	36	*	54
4266·286	5	3	117183·654	14·53	2·86	18	2·47776	14·3		53
					2·8	15	2·48392	14·0	*	54
4272·168	3	3	117151·387	14·52	3·68	5	2·58768	11·04		25
					7·55	20	2·27560	22·65		53
					7·1	15	2·30223	21·3	*	54
4300·100	5	3	116999·389	14·50	3·58	20	2·38062	17·9		53
					3·4	15	2·40302	17·0	*	54
4333·560	5	3	118469·117	14·69	4·9	25	2·24777	24·5	*	54
4335·3374	3	3	118459·662	14·69	4·0	25	2·55785	12·0		54
					3·33		2·63702	10·0	*	
4345·167	3	3	118407·494	14·68	2·8	15	2·71372	8·4	*	54
4510·7332	1	3	117563·020	14·57	10·2	20	2·64564	10·2	*	53
5558·7015	5		122086·974	15·14	8·3	25	2·12962	41·5		54
5572·548	7		123557·459	15·32	3·9	25	2·30987	27·3		54

contd./

(a)	(b)	(c)	(d)	(e)	(f)	(g)	(h)	(i)	(j)	(k)
5606•732	3		121932•908	15•12	15•0	25	2•09552	45•0		54
5650•703	1	3	121794•158	15•10	19•0	25	2•47337	19•0		54
6032•124	9	7	122036•134	15•13	21•0	25	1•50401	189		54
6052•721	5		120600•944	14•95	2•5	25	2•68506	12•5		54
6059•373	5		120619•076	14•95	3•8	25	2•50369	19•0		54
6965•4304	3	5	107496•463	13•33	53•1	6	1•64073	159•3		25
					54•1	10	1•63263	162•3		55
					54•0		1•63344	162•0		58
					87	~ 25	1•42631	261		61
7067•217	5	5	107289•747	13•30	53	~ 30	1•42599	265		61
7147•041	3	5	107131•755	13•28	~ 30	> 30	1•89989	90		61
7272•936	3		107496•463	13•33	161	5	1•17774	483		25
7383•980	5		107289•747	13•30	107	30	1•13994	535		19
					86•8	6	1•23081	434		25
					89	~ 25	1•21994	445		61
7471•18	3	3	107131•755	13•28	< 40	> 30	1•79421	120		61
7503•867	1	3	108722•668	13•48	550	30	1•13490	550	***	19
					432	4	1•23981	432		25
					314	10	1•37837	314		55
					406	4	1•26677	406		56
7514•6514	1		107054•319	13•27	480	30	1•19463	480	***	19
					362	7	1•31622	362		25
					296	10	1•40459	296		55
					383	4	1•29270	383		56
					301		1•37015	301		58
					520	~ 25	1•15991	520		61
7635•105	5	5	106237•597	13•17	250	30	0•78591	1250	**	19
					•203	4	0•87636	1015		25
					141	10	1•03463	705		55
					183	4	0•92142	915		56
					144	6	1•02547	720		58
					184	~ 25	0•91902	920		61
7723•760	3		106087•305	13•15	99•0	30	1•41510	297		19
					41	~ 30	1•79792	123		61
7724•206	3	1	107496•463	13•33	131	30	1•29569	393		19
					195	~ 30	1•12069	585		61

contd./

(a)	(b)	(c)	(d)	(e)	(f)	(g)	(h)	(i)	(j)	(k)
7948·175	3	1	107131·755	13·28	218	30	1·11901	654	***	19
					147	5	1·25592	441		25
					251	~ 25	1·02349	753		61
8006·156	5	3	106237·597	13·17	51·0	3	1·49688	255	***	25
					54	~ 25	1·47206	270		61
8014·786	5	5	105617·315	13·09	93·0	30	1·23644	465	***	19
					79·6	5	1·30401	398		25
					57·2	10	1·44752	286		55
					74·9	4	1·33042	374·5		56
					58·9		1·43481	294·5		58
					89	~ 25	1·25553	445		61
8103·6920	3	3	106087·305	13·15	243	30	1·04593	729	**	19
					268	5	1·00335	804		25
					148	10	1·26128	444		55
					194	4	1·14374	582		56
					153		1·24687	459		58
					184	~ 25	1·16673	552		61
8115·3108	7	5	105462·804	13·08	222	30	0·71786	1554	**	19
					222	6	0·71786	1554		25
					118	10	0·99233	826		55
					155	4	0·87387	1085		56
					122		0·97784	854		58
					194	~ 25	0·77645	1358		61
8264·521	3	3	107496·463	13·33	154	30	1·25257	462	***	19
					155	8	1·24975	465		25
					99·6	10	1·44039	299·8		55
					131	4	1·32281	393		56
					103		1·42727	309		58
8408·208	5	3	107289·747	13·30	188	30	0·95158	940	**	19
					199	5	0·92689	995		25
					117	10	1·15756	585		55
					155	4	1·03532	775		56
					122		1·13944	610		58
8424·6473	5	3	105617·315	13·09	167	30	1·00377	835	**	19
					194	5	0·93878	970		25
					105	10	1·20538	525		55
					139	4	1·08358	695		56
					109		1·18914	545		58
					107	~ 25	1·19720	535		61
8521·441	3	3	107131·755	13·28	106	3	1·42808	318	***	25
8667·943	3	1	106087·305	13·15	< 40	> 30	1·85874	120		61
9122·966	3	5	104102·144	12·91	95	~ 30	1·50529	285		61
9657·784	3	3	104102·144	12·91	~ 30	> 30	2·03064	90		61

Transition/

Transition Probability Data, Argon ArII

(a)	(b)	(c)	(d)	(e)	(f)	(g)	(h)	(i)	(k)
3545·58	6	4	187589·62	23·26	686		$\bar{1}$·93521	4116	55
3588·44	10	8	185093·92	22·95	194		0·26713	1940	55
					581		$\bar{1}$·78842	5810	58
3729·29	4	6	161049·65	19·97	203		0·66207	812	55
					119		0·89401	476	57
					626		0·17315	2504	58
3850·57	4	4	161049·65	19·97	28·4		1·52900	113·6	55
					54·4		1·24781	217·6	57
					88·3		1·03745	353·2	58
3928·62	4	2	161049·65	19·97	474		0·31643	1896	55
					174		0·75163	696	57
4013·87	8	8	157234·93	19·49	175		0·45744	1400	55
					550		$\bar{1}$·96010	4400	58
4348·11	8	6	157234·93	19·49	1150	5	$\bar{1}$·67451	9200	25
					927		$\bar{1}$·76812	7416	55
					1280		$\bar{1}$·62800	10240	57
4379·74	2	2	161090·31	19·97	1160	7	0·27596	2320	25
					1120		0·29117	2240	57
4401·02	6	8	155044·07	19·22	371		0·29603	2226	55
					1210		$\bar{1}$·78261	7260	58
4426·01	6	4	157674·30	19·55	1150		$\bar{1}$·80716	6690	55
					871		$\bar{1}$·90361	5226	57
4430·18	4	2	158168·71	19·61	857		0·11144	3428	55
					621		0·25128	2484	57
4579·39	2	2	161090·31	19·97	744	5	0·48821	1488	25
					10		2·35979	20	57
4589·93	6	4	170401·88	21·12	640	4	0·07752	3840	25
					615		0·09480	3680	55
					1000		$\bar{1}$·88365	6000	57
					2020		$\bar{1}$·57831	12120	58
4609·60	8	6	170531·29	21·14	906	5	$\bar{1}$·80343	7248	25
					1070		$\bar{1}$·73119	8560	57
4637·25	6	6	170401·88	21·12	64	5	1·08188	384	25
					58·3		1·12244	349·8	55
					81		0·97963	486	57
					193	14	0·60254	1158	58
4657·94	2	4	159707·46	19·80	695	10	0·52517	1390	25
					11		2·32573	22	57

contd./

(a)	(b)	(c)	(d)	(e)	(f)	(g)	(h)	(i)	(k)
4764.89	4	2	160240.35	19.87	540	12	0.34358	2160	25
					343		0.54070	1372	55
					709		0.22534	2836	57
					1140		0.01907	4560	58
4806.07	6	6	155044.07	19.22	786	3	0.00817	4716	25
					579		0.14095	3474	55
					788		0.00707	4728	57
					1930		$\bar{1}$.61808	11580	58
4847.90	2	4	155709.02	19.30	95	8	1.40679	190	25
					81		1.47603	162	57
4879.90	6	4	158731.20	19.68	659	4	0.09140	3954	25
					283		0.45847	1698	55
					771		0.02317	4626	57
					950		$\bar{1}$.93253	5700	58
4933.24	4	4	155352.04	19.26	160	7	0.88965	640	25
					241		0.70905	964	57
5009.35	6	4	155049.07	19.22	170	5	0.69118	1020	25
					122		0.83528	732	55
					139		0.77861	834	57
					413		0.30566	2478	58
5062.07	4	2	155352.04	19.26	220	5	0.75985	880	25
					281		0.65355	1124	57

APPENDIX III/

APPENDIX III

Best Straight Line through a given Set of Points

The best straight line which can be drawn through a series of n points $(x_1,y_1) \ldots (x_i,y_i) \ldots (x_n,y_n)$ is defined as the line such that the sum of the squares of the perpendicular distances of the points from the line is a minimum. (For a general treatment of the method of least squares, see Ref. 60.) We have to determine the gradient only of the line, this being inversely proportional to the temperature.

Thus, if the equation of the line be $y = mx + c$, and bearing in mind that the gradient m is of the order 10^{-4}, we have for the perpendicular distance p_i from the point (x_i,y_i) to the line:

$$p_i = y_i - mx_i - c$$

$$\therefore p_i^2 = y_i^2 + m^2x_i^2 + c^2 - 2mx_iy_i - 2cy_i + 2mcx_i$$

$$\therefore \Sigma p_i^2 = \Sigma y_i^2 + m^2\Sigma x_i^2 + nc^2 - 2m\Sigma x_iy_i - 2c\Sigma y_i + 2mc\Sigma x_i. \quad \ldots(A.III.1)$$

Now, for Σp_i^2 to be a minimum, we have the condition:

$$\frac{\partial}{\partial x}(\Sigma p_i^2) = 0$$

$$\therefore \frac{\partial}{\partial x}(\Sigma p_i^2) = m\Sigma x - \Sigma y + cn = 0. \quad \ldots(A.III.2)$$

Partial differentiation with respect to y yields the same result.

Thus, by taking our original equation $y = mx + c$ and substituting summed co-ordinates for the existing co-ordinates, we have the equation (A.III.2) which satisfied our condition for the "best straight line".

$$\Sigma y = m\Sigma x + nc. \quad \ldots(A.III.2a)$$

Taking our original equation in the form

$$xy = mx^2 + cx$$

and substituting summed co-ordinates, we have

$$\Sigma xy = m\Sigma x^2 + c\Sigma x. \quad \ldots(A.III.3)$$

Thus, solving (A.III.2a) and (A.III.3) simultaneously, we have

$$m = \frac{n\Sigma xy - \Sigma x\Sigma y}{n\Sigma x^2 - (\Sigma x)^2} \quad \ldots(A.III.4)$$

and/

and, incidentally,
$$c = \frac{\Sigma y \Sigma x^2 - \Sigma x \Sigma xy}{n\Sigma x^2 - (\Sigma x)^2}. \qquad \ldots(A.III.4a)$$

Now, in our case, we have

$$x = E_m$$

and
$$y = \log_{10}\left(\frac{I\lambda}{gA}\right)$$

and clearly, if a particular set of n abscissae (i.e., the same n spectral lines) are employed in each temperature determination, then the denominator of equation (A.III.4) will remain constant and it will only be necessary to evaluate Σy and Σxy each time.

The standard deviation of the points from the line is defined as

$$\sigma^2 = \frac{\Sigma p_1^2}{n} \qquad \ldots(A.III.5)$$

and thus σ may be readily evaluated from equation (A.III.1), always working to ten significant figures.

A variety of criteria exist to connect this standard deviation σ with the deviation from the measured gradient σ_m, and of these, the following two extremes (A.III.6) and (A.III.7) will be seen to quite reasonably include the scatter of our temperature measurements (see Figs. 12 and 13).

Setting
$$\frac{\sigma}{\bar{y}} = \frac{\sigma_m}{m} \qquad \ldots(A.III.6)$$

where σ is given by equation (A.III.5)

$\bar{y}$ is the mean value of the ordinate

σ_m is the deviation of the gradient

and m is the measured gradient,

we obtain an error σ_m/m of the order 1%.

On the other hand, considering the "maximum possible error", if the line AB be $y = mx + c$ (Fig. 14), then the line CD, constructed by putting AC = BD = $\frac{2}{3}\sigma$,* has gradient $(m + \sigma_m)$. From this construction, it can be seen that

$$\sigma_m = \frac{4\sigma}{3\Delta x} \qquad \ldots(A.III.7)$$

where Δx = extreme range of values of x co-ordinates. Equation (A.III.7) gave errors of the order 10 - 15% in most cases.

---

*$\frac{2}{3}\sigma$ is defined as the "Probable Error"; erf (0·67) = 50%.

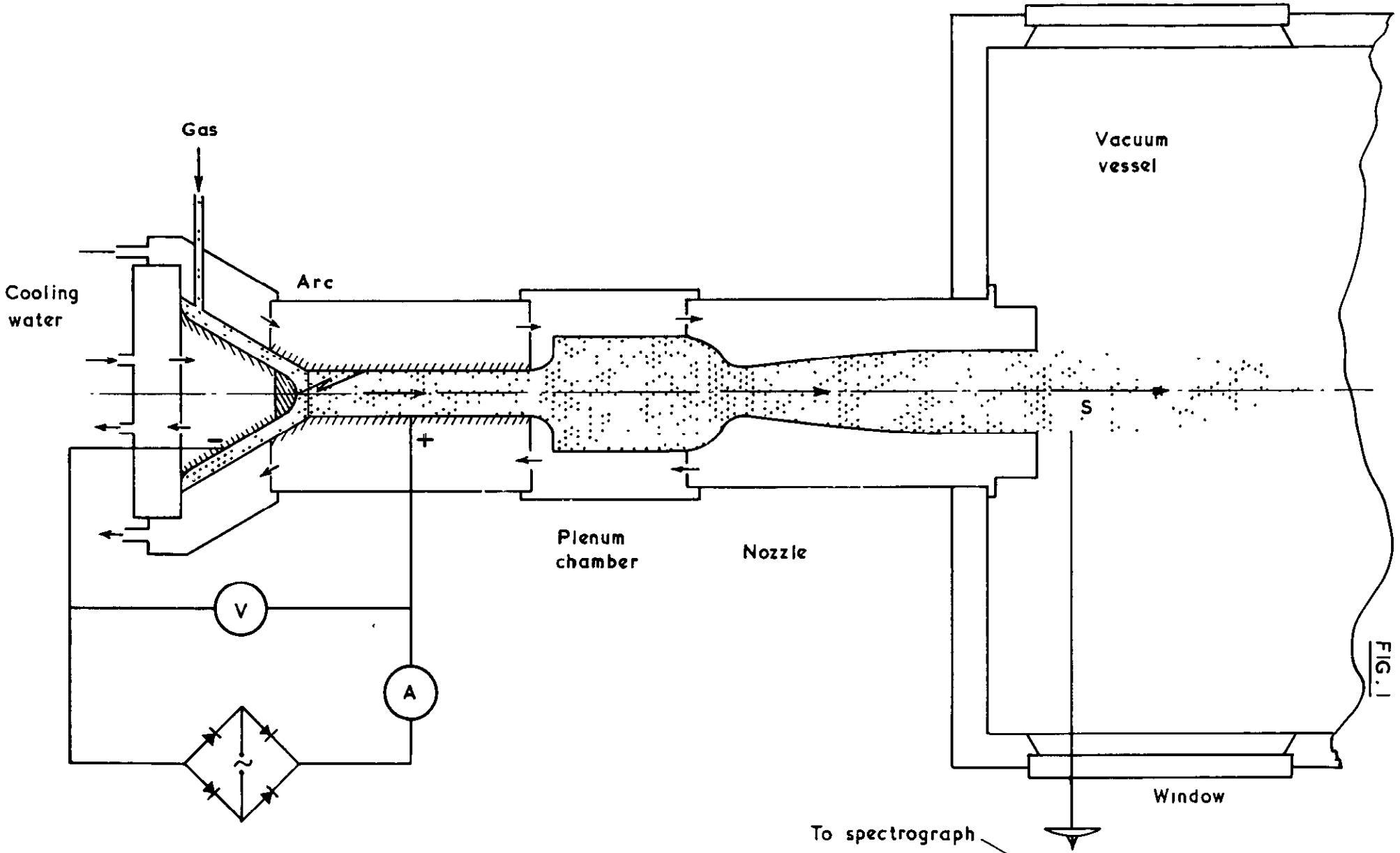

FIG. 1

This shows the arrangement of the electrodes and nozzle of the Plasma – jet Wind Tunnel at Imperial College. The region in the jet from which the analysed radiation was emitted, is shown at the nozzle exit (S).

FIG. 2

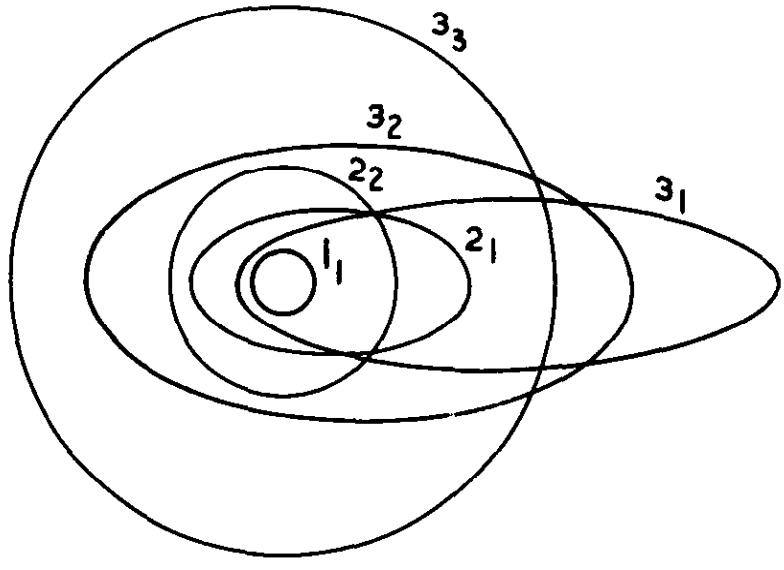

A simple representation of electron orbits in an atom of a light element

Figure reproduced by courtesy of J. Yarwood

FIG. 3

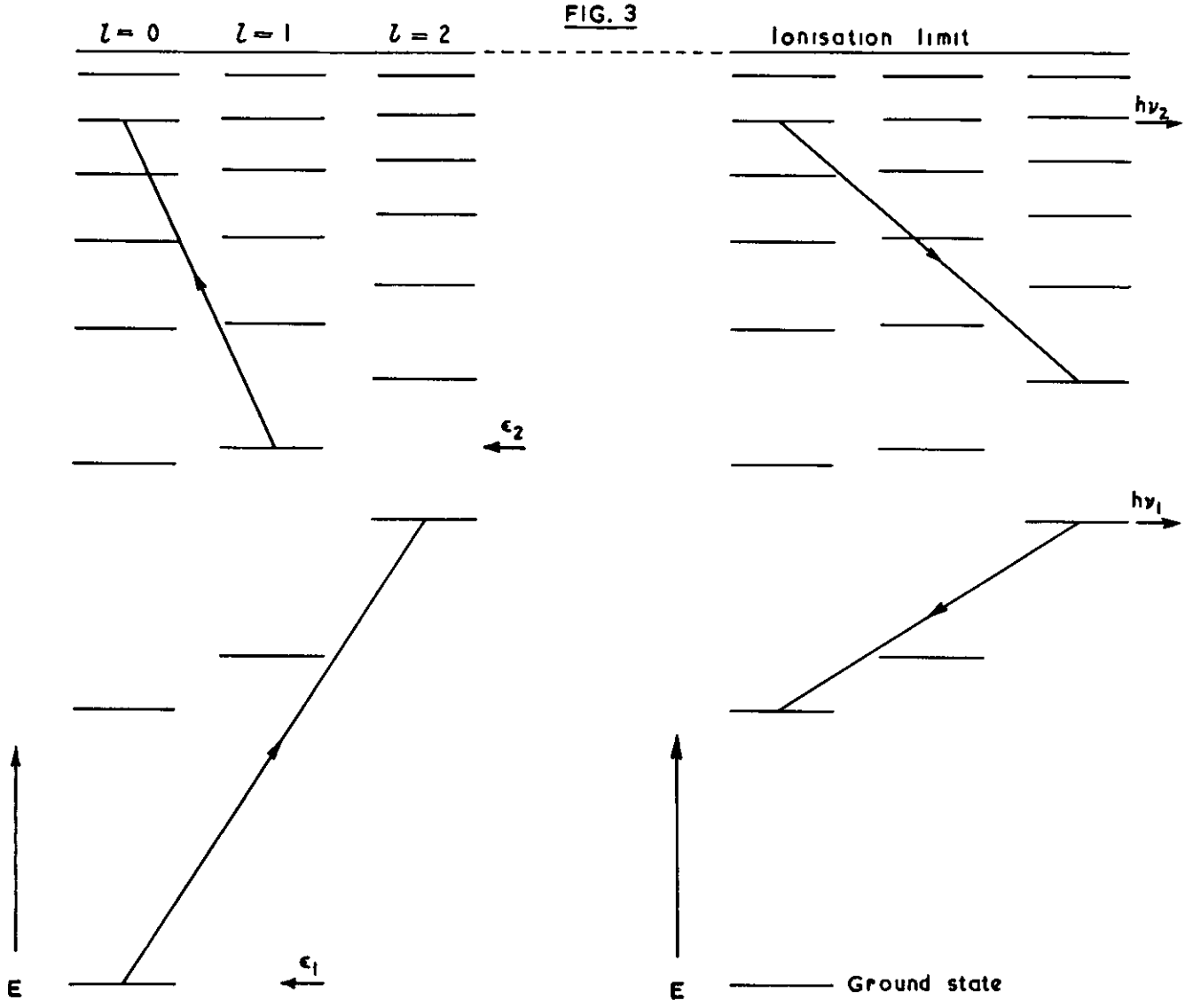

Transitions occuring in an excited atom.

On the left: two transitions are shown which occur as a result of the absorption of two distinct quantities of energy, ϵ_1 and ϵ_2. On the right: two photons of different energies, $h\nu_1$ and $h\nu_2$, are emitted as the result of the electrons in the upper levels returning to two vacant lower levels. Each photon would contribute to the light of the corresponding individual spectral lines

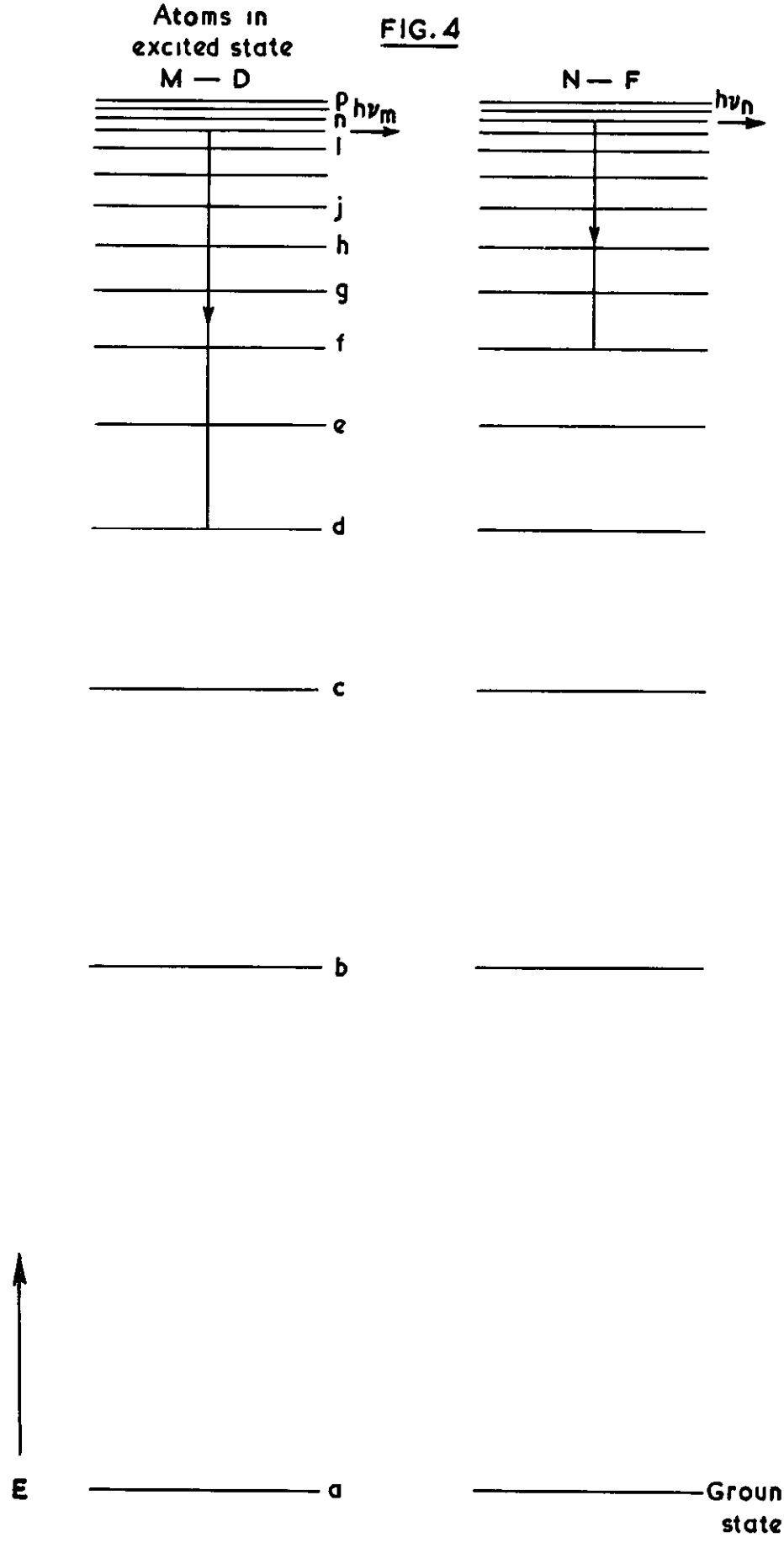

FIG. 4

This represents the energy levels of two atoms of the same element (the different values of l are neglected, all energy levels are shown in one column only). The transitions shown occurring in these atoms are those discussed in the text, Sec. 4·3, i.e. M — D and N — F.

FIG. 5

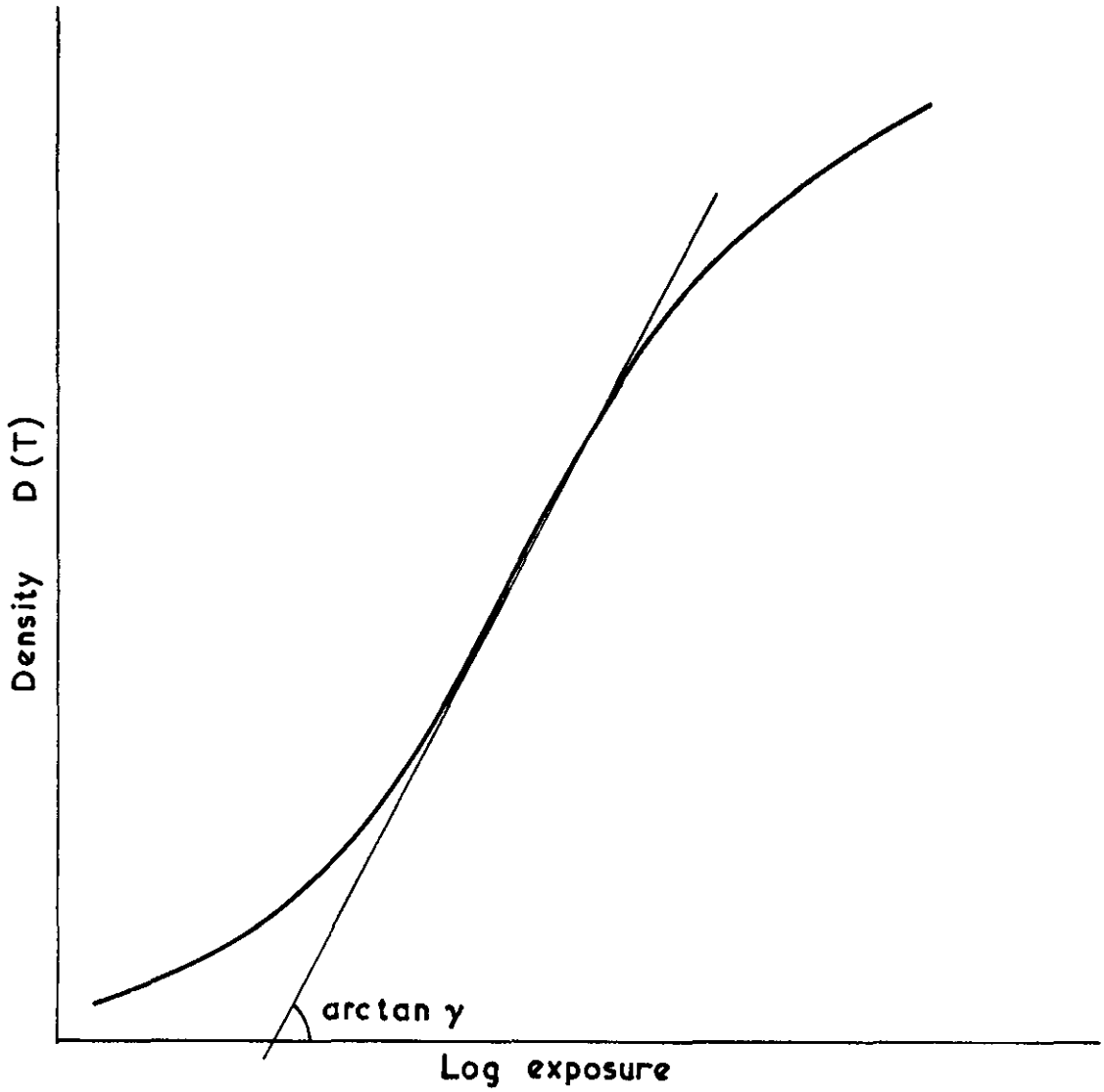

A typical 'characteristic (density) curve', indicating the significance of γ, see Sec. 5·32

FIG. 6

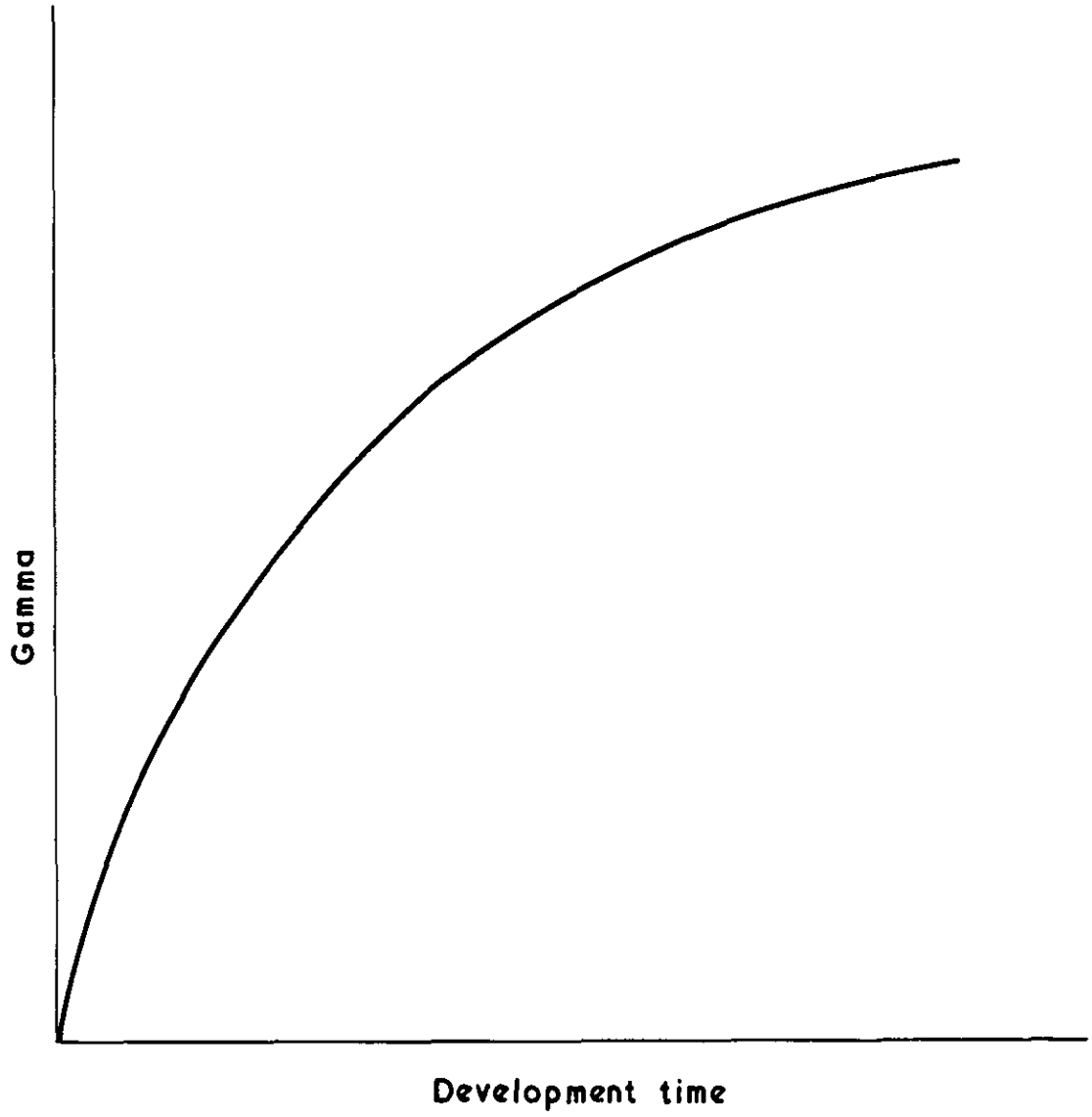

The variation of contrast (γ) with development time

FIG. 7

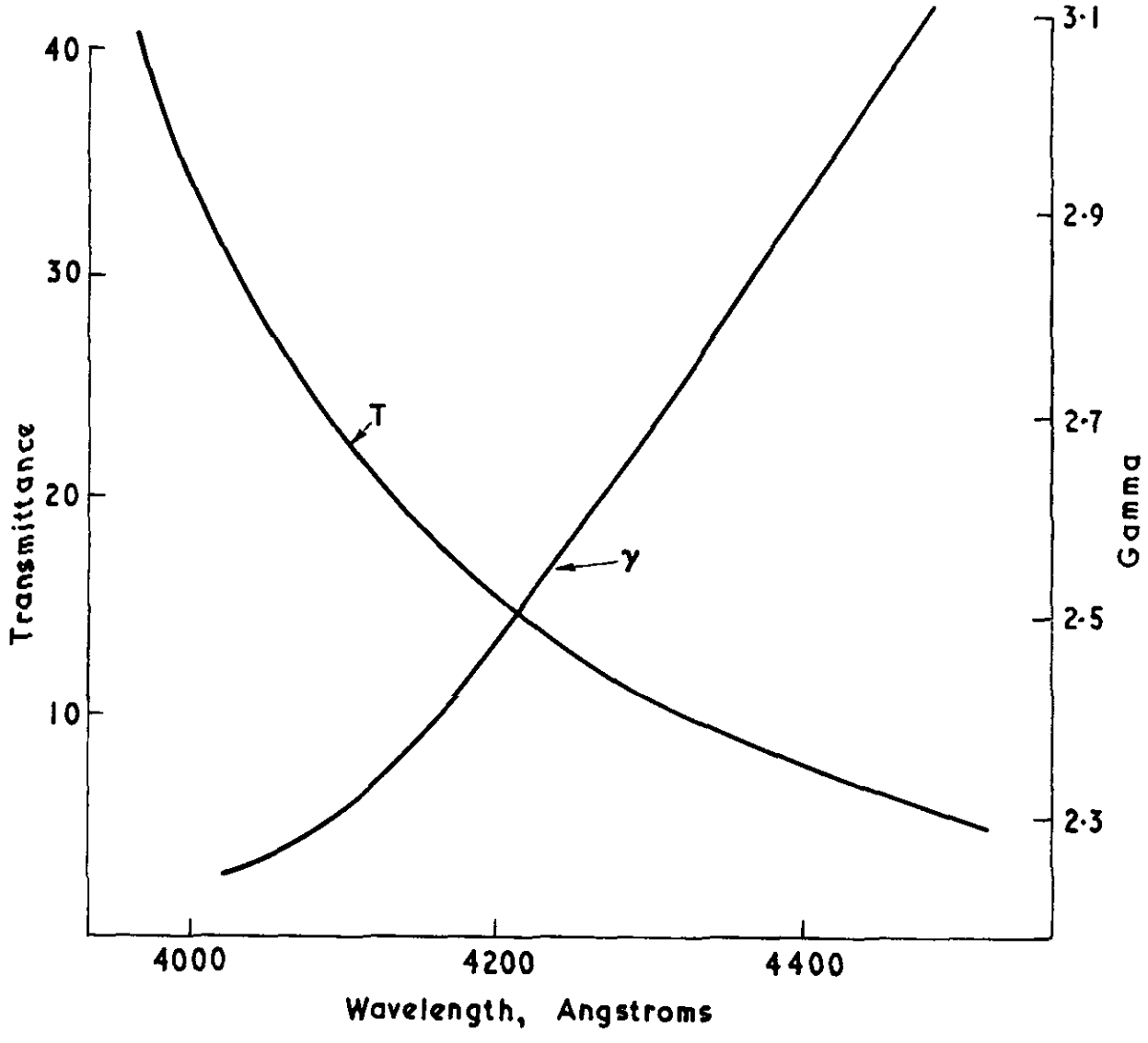

The variation of transmittance and contrast (γ) with wavelength. Derived from the densitometer trace of a standard lamp continuum spectrogram

FIG. 8

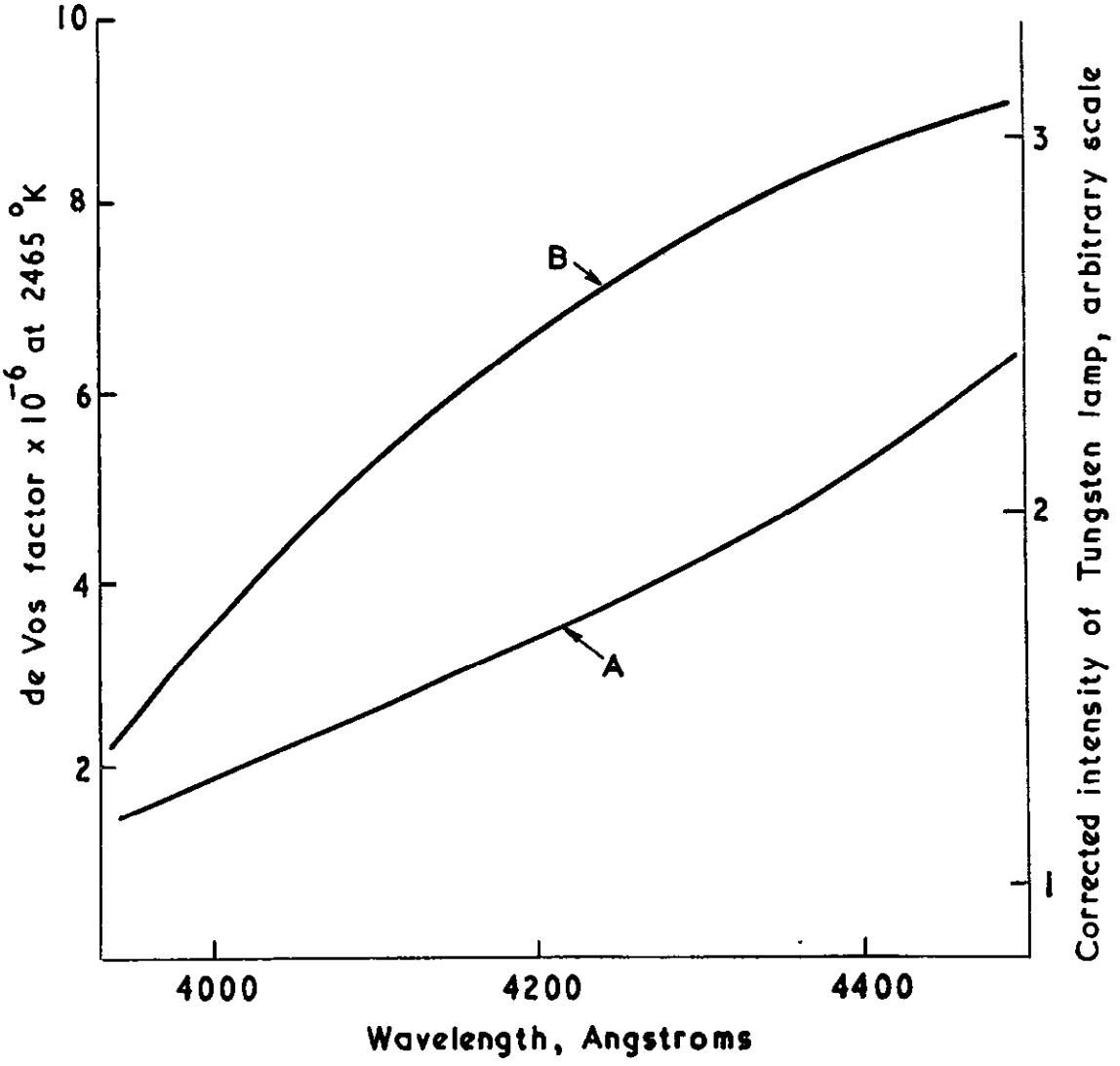

Curves employed in computing the colour calibration characteristics of an emulsion:

(A) the tungsten emissivity characteristic

(B) the actual variation of the continuum intensity at the plate

Diagram by courtesy of 'Bausch and Lomb, Inc'

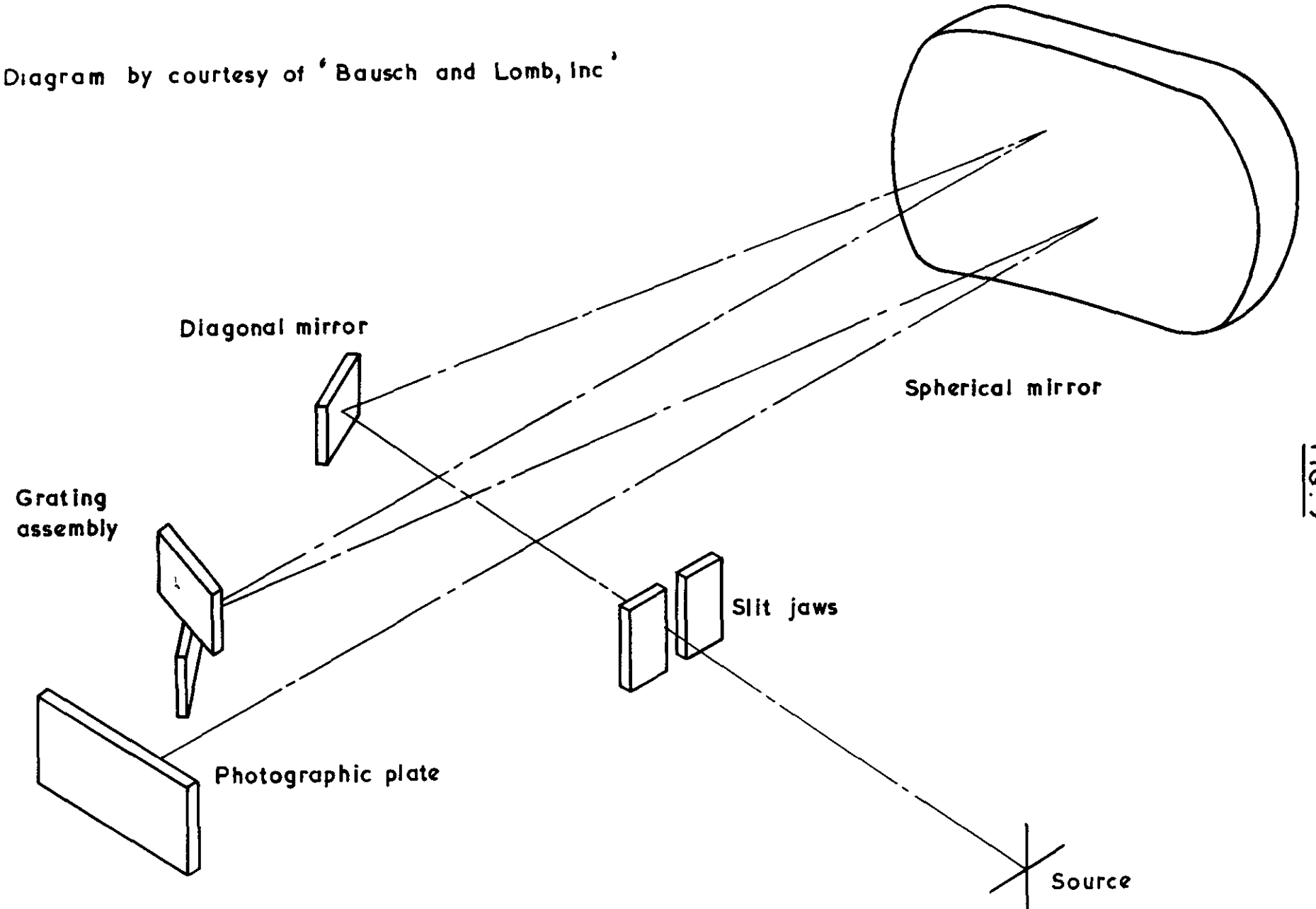

FIG. 9

The optical system and the path of light in the 'Dual grating spectrograph'

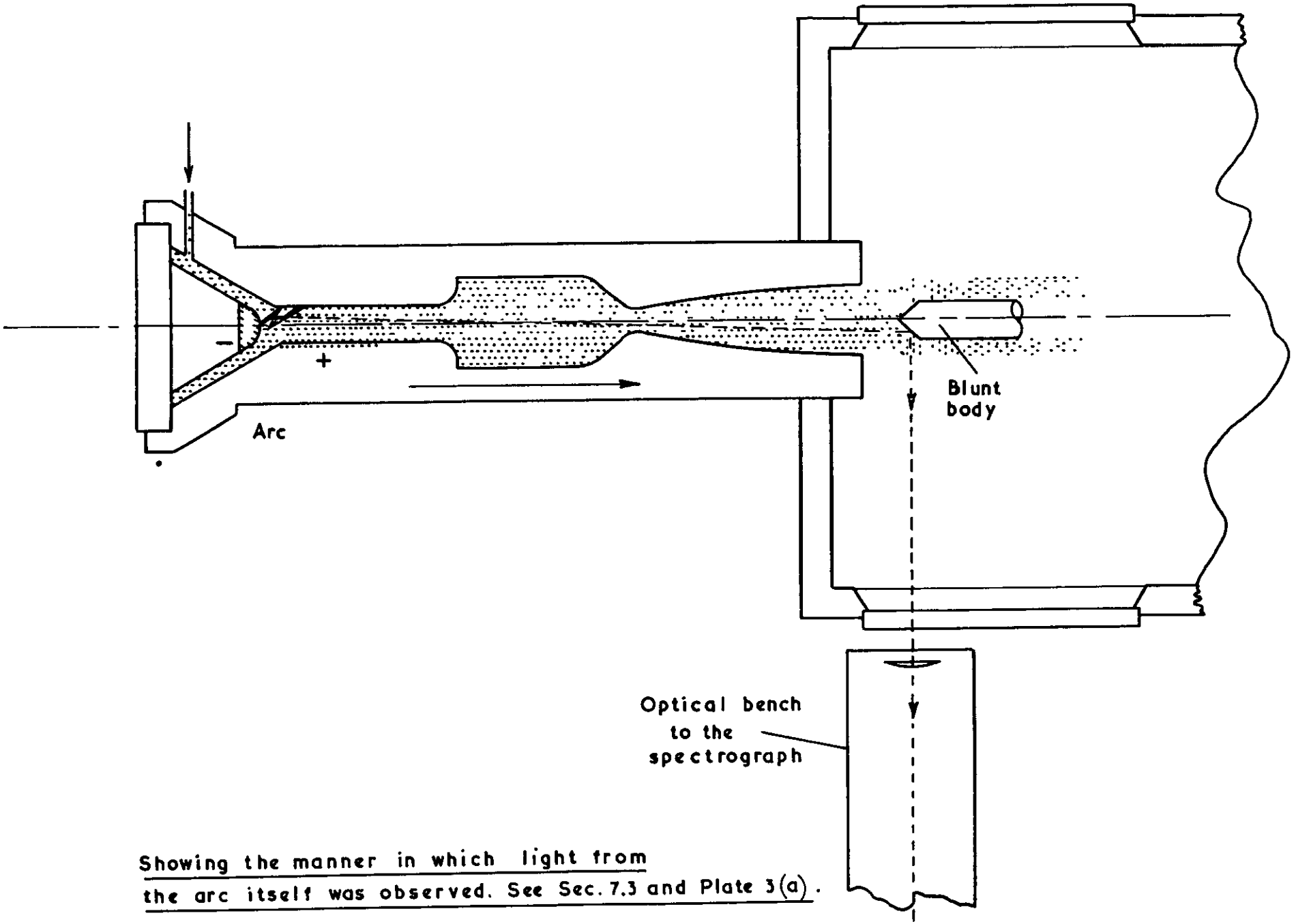

FIG. 10

Showing the manner in which light from the arc itself was observed. See Sec. 7.3 and Plate 3(a).

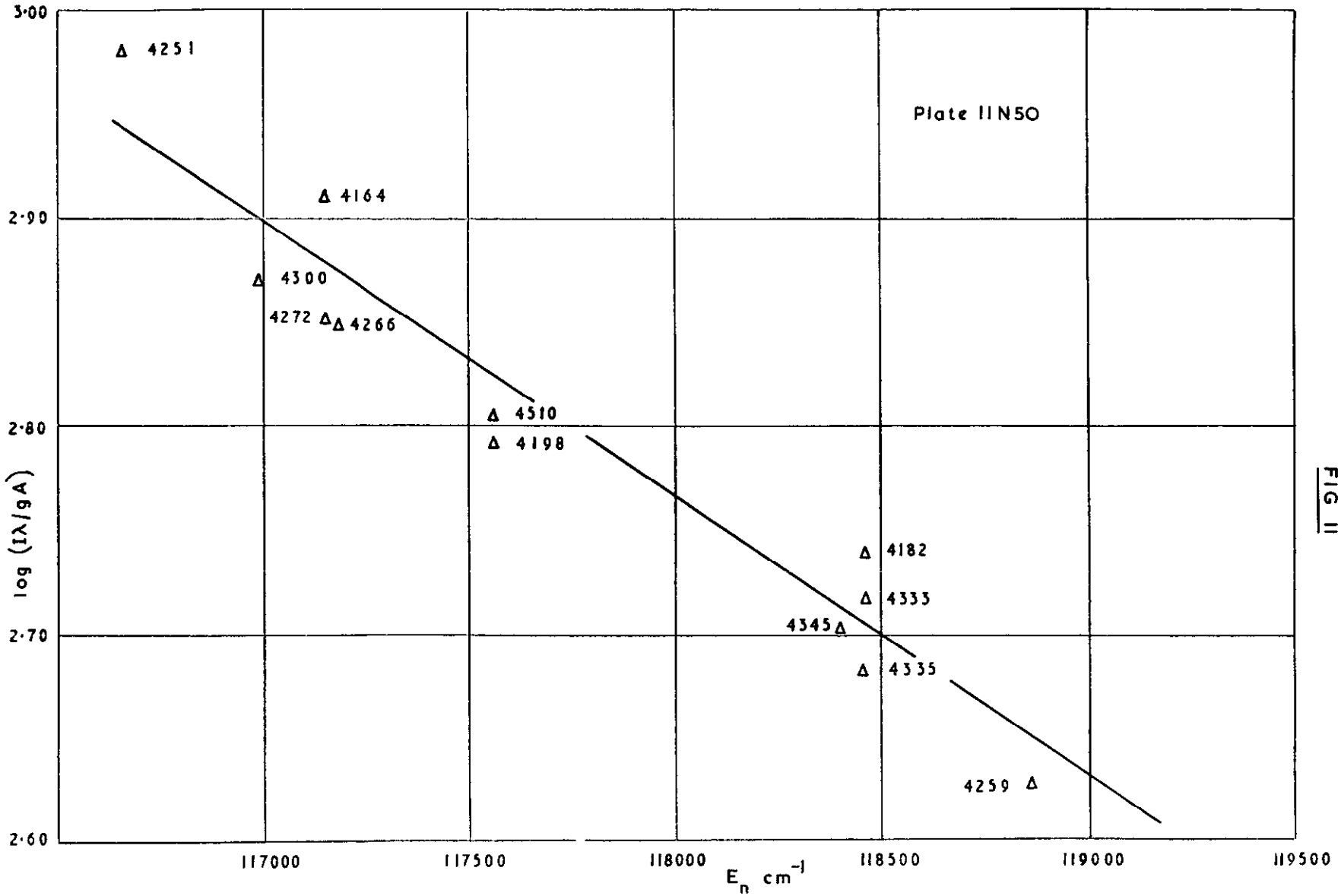

FIG II

A typical plot of $\log_{10}(I\lambda/gA)$ against E_n The numbers adjacent to the points indicate the wavelengths of the argon lines concerned. The statistically derived gradient for the best-fit straight line is $1{\cdot}349 \cdot 10^{-4}$ cm. The line which has been drawn in this plot is an indication of the position of the statistical result. The temperature corresponding to this gradient is 4,630° K

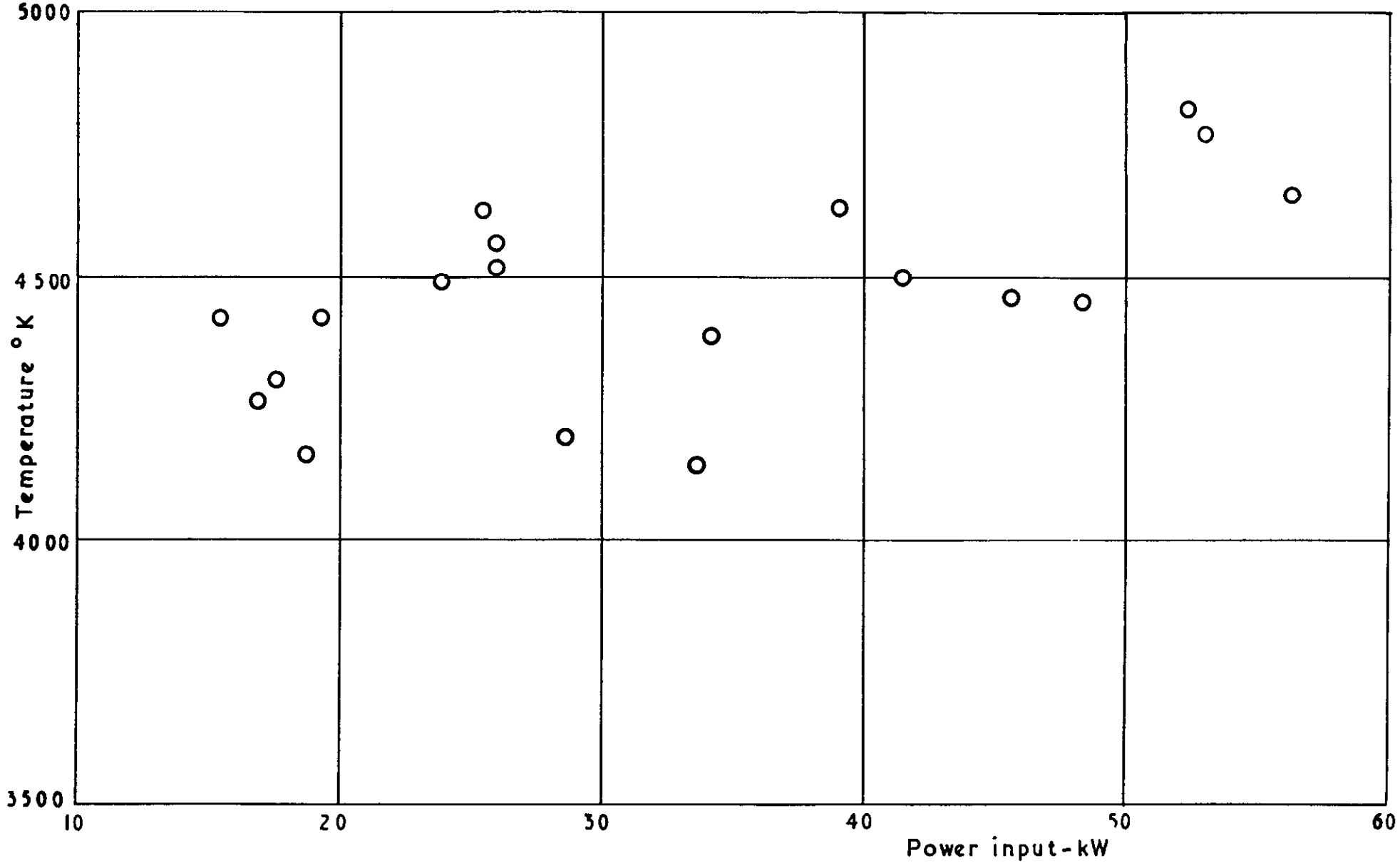

FIG. 12

Experimental plot of the variation of the measured excitation temperatures with power input to the electrodes. The argon mass flow rate was constant at 70·3 g min^{-1} (0·155 lb min^{-1})

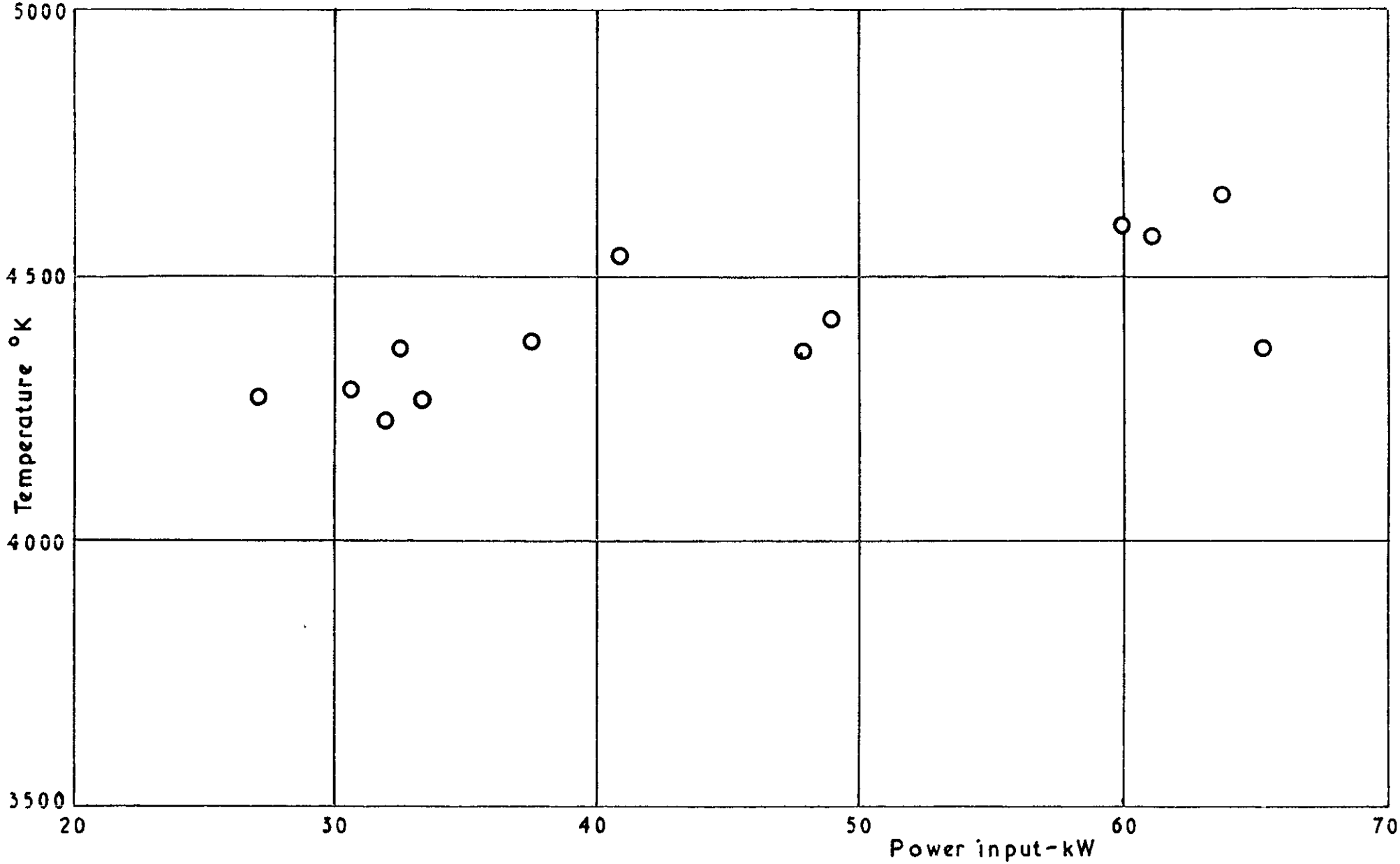

FIG. 13

As for Figure 12, but argon mass flow rate now constant at 99·0 g min^{-1} (0·218 lb min^{-1})

FIG. 14

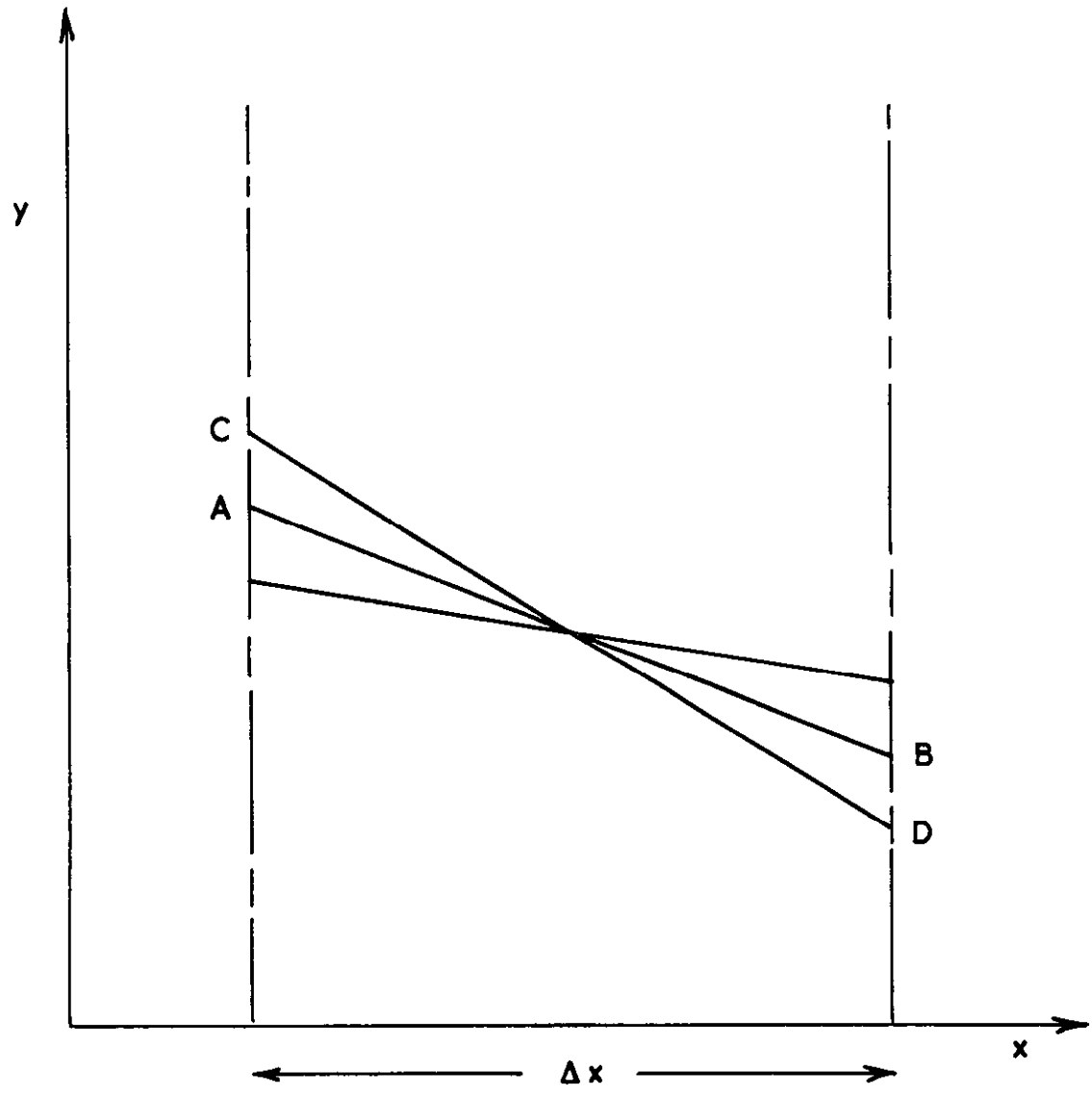

Graph illustrating the 'maximum possible error' criterion, see Sec. 15.

FIG. 15

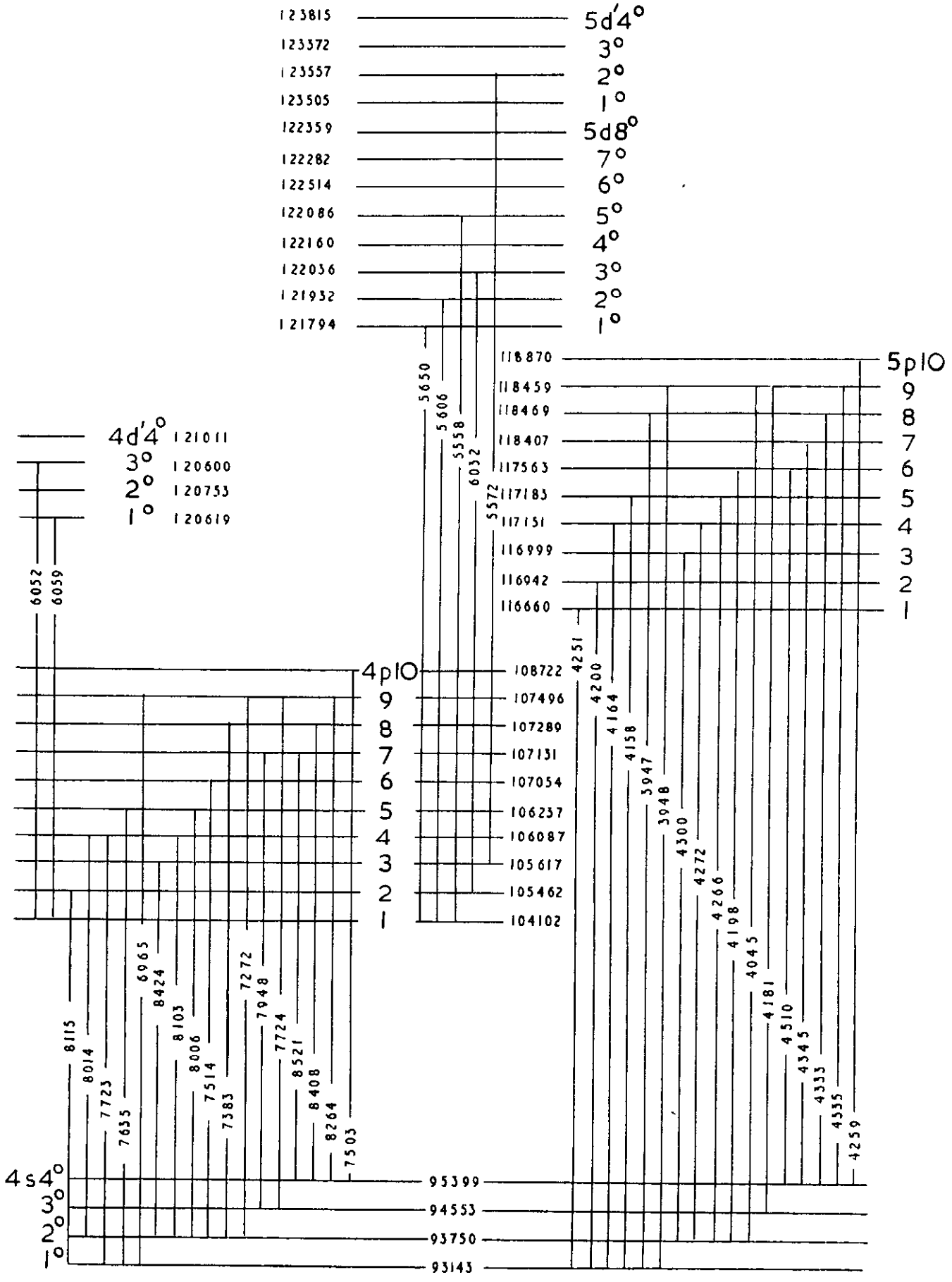

Energy level diagram for Ar I multiplets.

FIG. 16

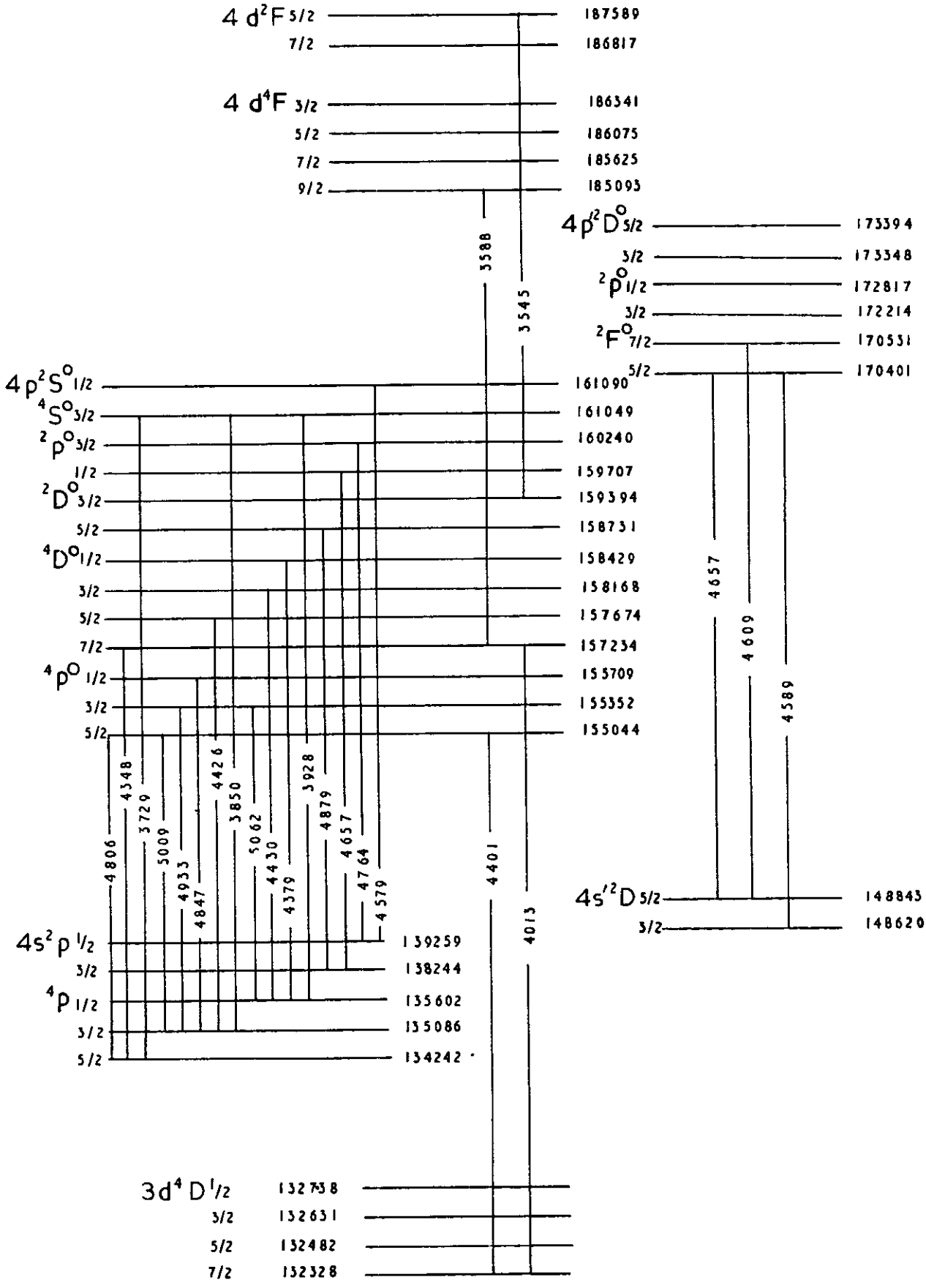

Energy level diagram for Ar II multiplets; the 'd' levels are incomplete.

PLATE I

The arc-heated wind tunnel and its control panel. The spectrograph can be seen on the left, mounted on an anti-vibration concrete block.

PLATE 2

The Bausch & Lomb "Dual Grating" spectrograph, mounted on its transportation trolley.

PLATE 3

Six spectrograms from a medium glass spectrograph, showing the radiation emitted from the plasma jet within the spectral range 3,980A to 4,540A, operating with argon at 15 kW. These exposures were taken with a water-cooled blunt body placed in the jet at the nozzle exit (see Fig. 10).

(a) Ar I and Ar II lines - emission from the arc, reflected by the body, exposure 30 s.

(b) Ar I lines from the free stream just ahead of the shock front, exposure 60 s.

(c) As (b), but further upstream, exposure 90 s. The argon blue lines discussed in this paper, are indicated by white dots below this spectrogram.

(d) As (a), exposure 60 s.

(e) Ar I and Ar II lines from the stagnation region between the body and the shock front, exposure 240 s.

(f) As (e), exposure 180 s.

PLATE 4

A spectrogram from the Bausch & Lomb "Dual Grating" spectrograph with the step-filter attached. A 1000 micron slit was used in this case, and serves to demonstrate that higher dispersion is required when wide slits are used. The 50 μm images of the argon blue lines normally used for this experiment just appear at the top of this plate. Exposure 8 s, 32 kW.

PLATE 5

Spectrogram from a Zeiss medium quartz spectrograph, with the plasma-jet operating on argon at 21 kW, this reproduction being on the same scale as Plate 4. The prominent argon blue group shown in Plate 4 appears on the right hand side of this spectrogram. The second positive nitrogen bands emitted from the surrounding low-pressure atmosphere (5 torr) are seen clearly, together with the CuI lines at 3,247 A and 3,273 A.

PLATE I

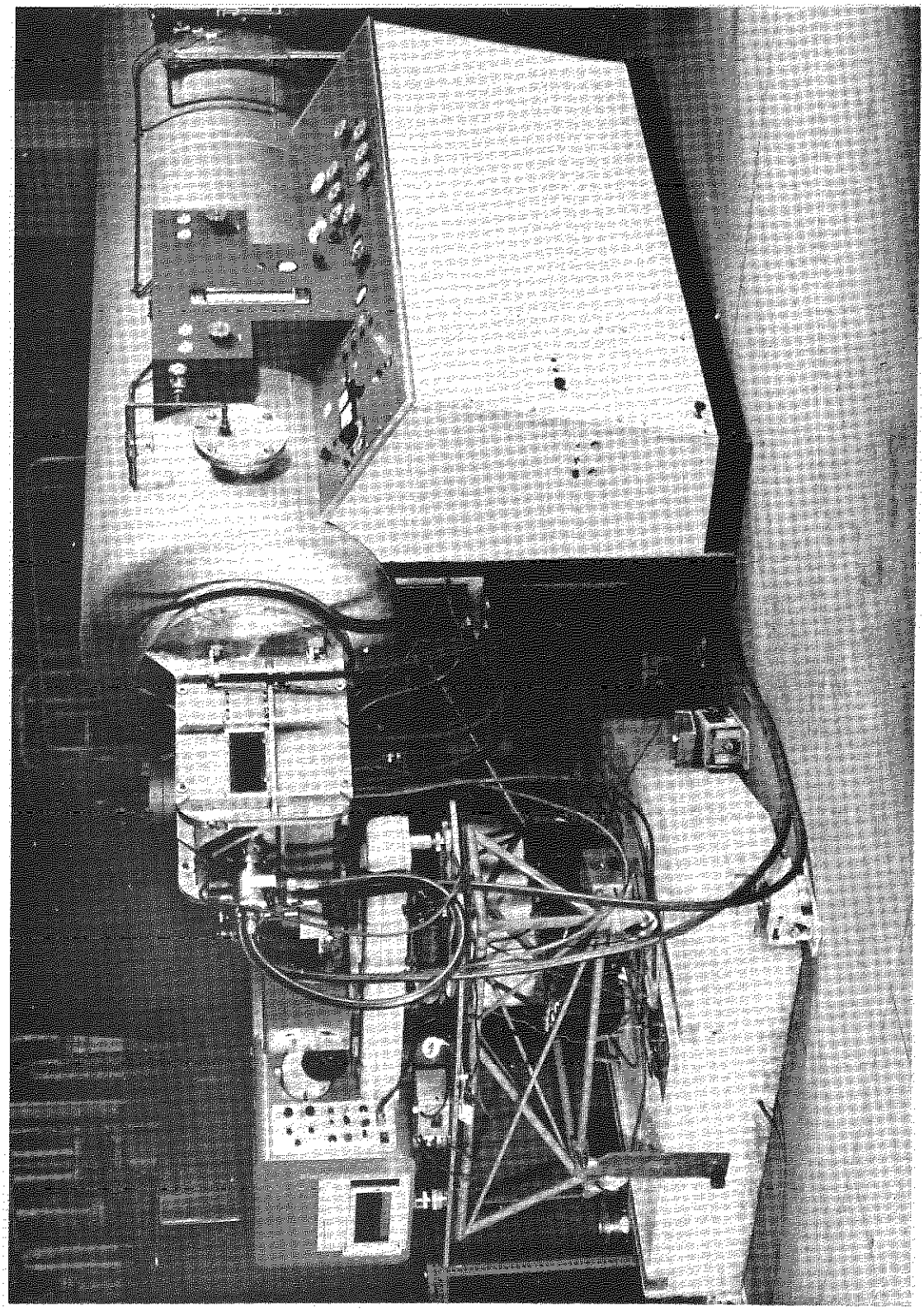

PLATE 2

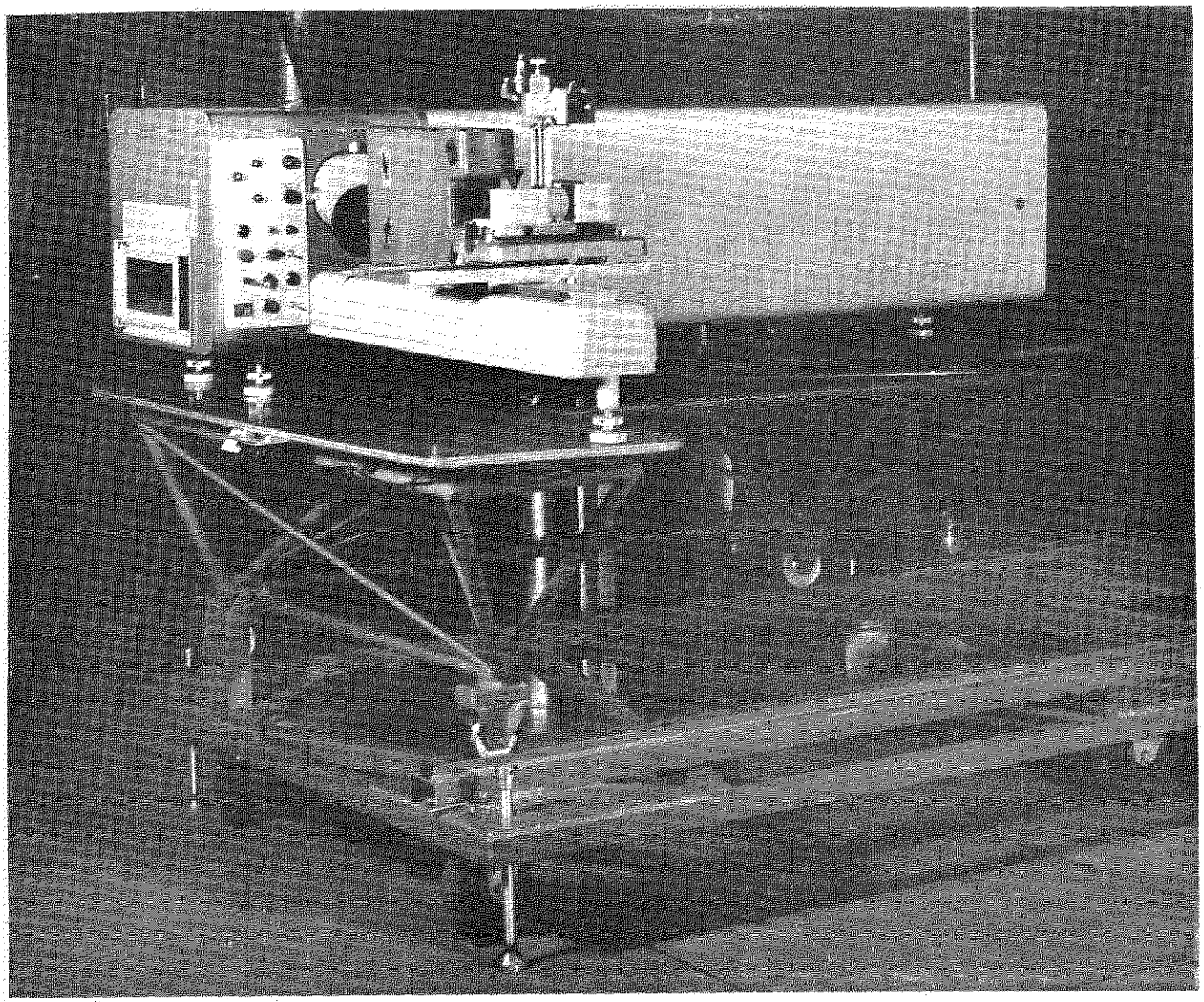

PLATE 3

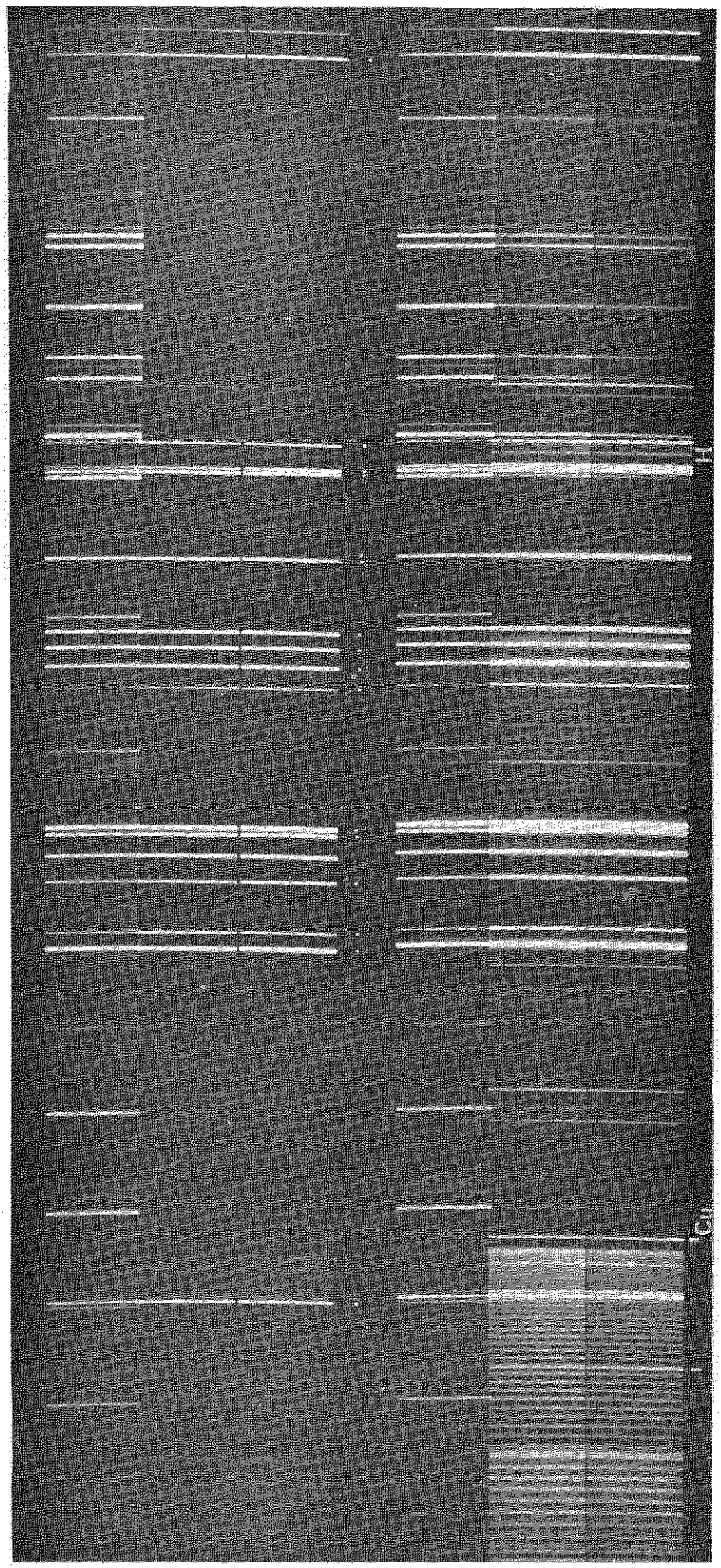

PLATES 4 & 5

PLATE 4

PLATE 5

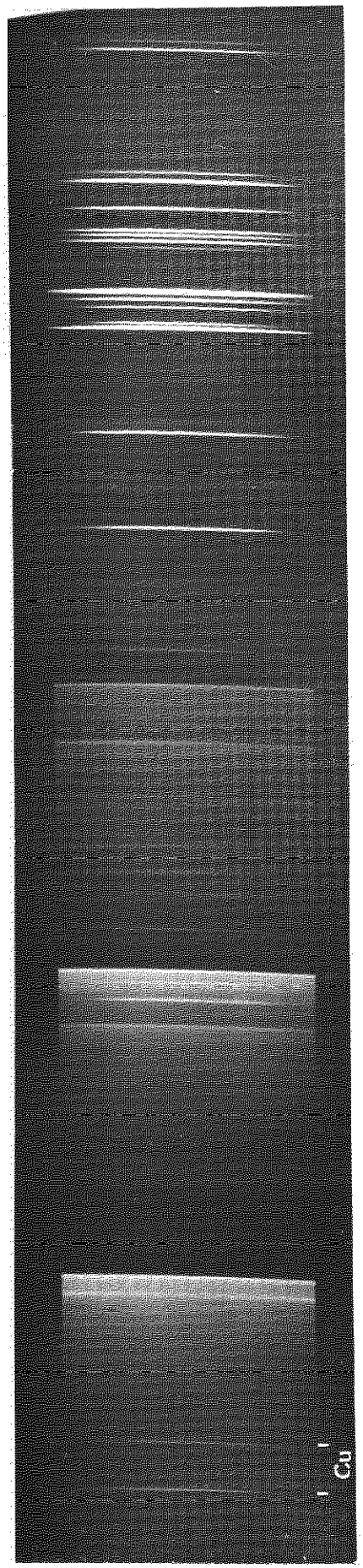

PLATE 6

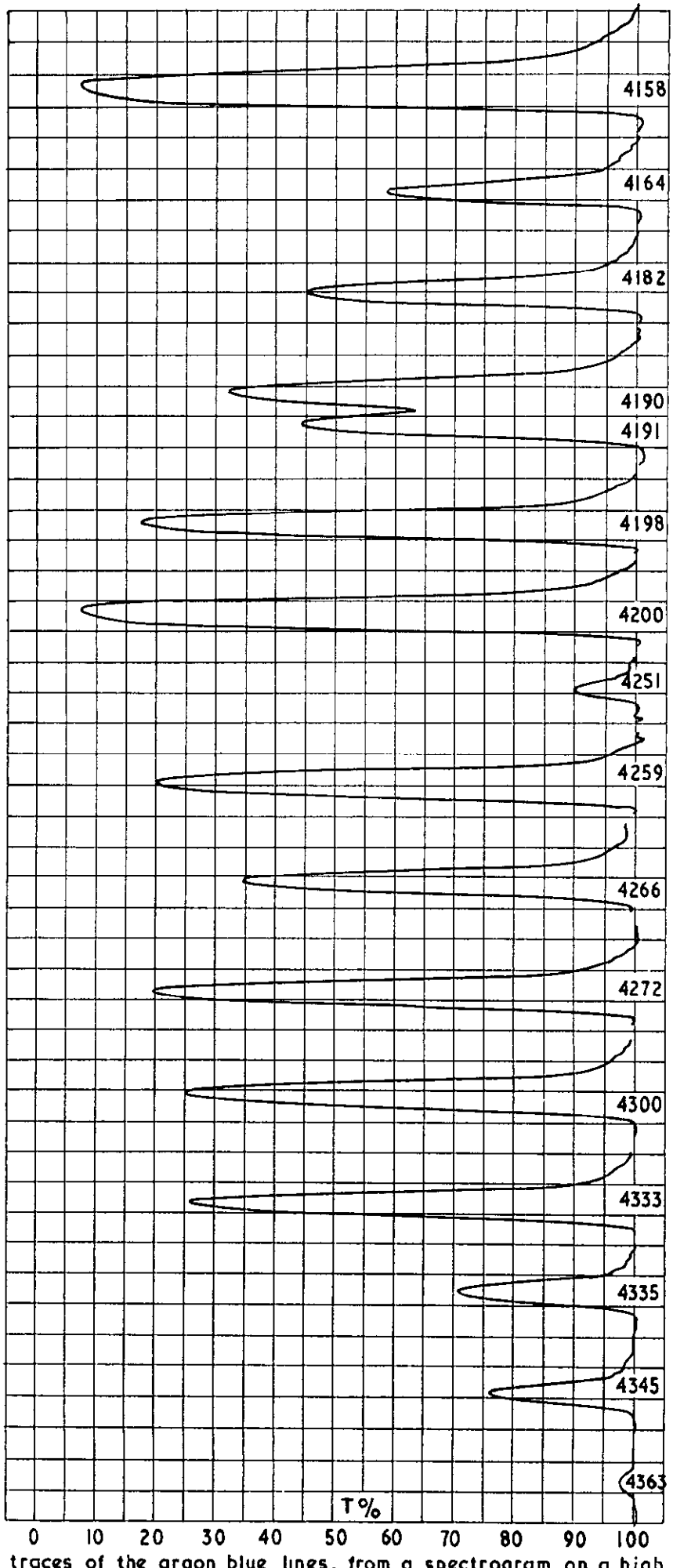

Densitometer traces of the argon blue lines, from a spectrogram on a high contrast plate showing a typical range of relative intensities

A.R.C. C.P. No.701
April, 1963
Adcock, B. D. and Plumtree, W. E. G., Imperial College

EXCITATION TEMPERATURE MEASUREMENTS OF GASES IN AN ARC-HEATED WIND TUNNEL AT $1{\cdot}3 \times 10^{-2}$ ATMOSPHERE, USING RELATIVE INTENSITIES OF SPECTRAL LINES

A description is given of a method for obtaining temperatures of gases by spectrogrammetric measurements of the relative intensities of spectral lines, applied to the gas in an arc-heated wind tunnel ('plasma-jet').

Qualitative details of impurities present in the wind tunnel are discussed.

An explanation starting from basic principles, concerning line spectra and relative intensity measurements, is designed for the benefit of technologists having only a general background knowledge of physics.

A comprehensive compilation of transition probabilities and other relevant data for neutral and first-stage ionization argon lines, is included as an Appendix.

A.R.C. C.P. No.701
April, 1963
Adcock, B. D. and Plumtree, W. E. G., Imperial College

EXCITATION TEMPERATURE MEASUREMENTS OF GASES IN AN ARC-HEATED WIND TUNNEL AT $1{\cdot}3 \times 10^{-2}$ ATMOSPHERE, USING RELATIVE INTENSITIES OF SPECTRAL LINES

A description is given of a method for obtaining temperatures of gases by spectrogrammetric measurements of the relative intensities of spectral lines, applied to the gas in an arc-heated wind tunnel ('plasma-jet').

Qualitative details of impurities present in the wind tunnel are discussed.

An explanation starting from basic principles, concerning line spectra and relative intensity measurements, is designed for the benefit of technologists having only a general background knowledge of physics.

A comprehensive compilation of transition probabilities and other relevant data for neutral and first-stage ionization argon lines, is included as an Appendix.

A.R.C. C.P. No.701
April, 1963
Adcock, B. D. and Plumtree, W. E. G., Imperial College

EXCITATION TEMPERATURE MEASUREMENTS OF GASES IN AN ARC-HEATED WIND TUNNEL AT $1{\cdot}3 \times 10^{-2}$ ATMOSPHERE, USING RELATIVE INTENSITIES OF SPECTRAL LINES

A description is given of a method for obtaining temperatures of gases by spectrogrammetric measurements of the relative intensities of spectral lines, applied to the gas in an arc-heated wind tunnel ('plasma-jet').

Qualitative details of impurities present in the wind tunnel are discussed.

An explanation starting from basic principles, concerning line spectra and relative intensity measurements, is designed for the benefit of technologists having only a general background knowledge of physics.

A comprehensive compilation of transition probabilities and other relevant data for neutral and first-stage ionization argon lines, is included as an Appendix.

Printed and published by
HER MAJESTY'S STATIONERY OFFICE
To be purchased from
York House, Kingsway, London w c 2
423 Oxford Street, London w 1
13A Castle Street, Edinburgh 2
109 St Mary Street, Cardiff
39 King Street, Manchester 2
50 Fairfax Street, Bristol 1
35 Smallbrook, Ringway, Birmingham 5
80 Chichester Street, Belfast 1
or through any bookseller

Printed in England

S.O. Code No. 23-9015-1